Design of an Experiment to Evaluate High-Power Rockets as a CubeSat Qualification Platform

Author: Peter Tanner

Supervisor: Dilusha Silva

ATTENTION: THIS IS A DRAFT VERSION. TODO: CHECK CHECKLIST BEFORE SUBMITTING *This thesis is presented in partial fulfilment of the requirements for the degree of Bachelor of Philosophy (Honours) at the University of Western Australia*

Faculty of Engineering and Mathematical Sciences

Word count: TODO:
Submitted: October 18, 2024

1 TODO: (!! REMOVE BEFORE FINAL RELEASE !!)

- `[ ]` Add schematics and PCB gerbers to appendix using `pdfpages`
- `[ ]` Add links to source repository `https://git.petertanner.dev/hpr-evaluation/`
- `[ ]` Use LaTeXtemplate for Honours papers
- `[ ]` Resolve all warnings except badness warnings because I don't know how to control that
- `[ ]` Make BibTeX consistent
- `[ ]` Bad citation format for datasheets and websites (Date is after access date).
- `[ ]` Check grammar and spelling
- `[ ]` Check presentation/typesetting
- `[ ]` Resolve all `TODO:` comments
- `[ ]` Finish all items on this checklist

Wts

- PROJECT BODY (ASSUME EXPERIMENTAL PROJECT)
  - 20% INTRODUCTION AND LITERATURE REVIEW
  - 15% EXPERIMENTAL DESIGN
  - 35% RESULTS AND DISCUSSION
- 10% CONCLUSION AND FUTURE WORK
- 10% SCOPE
- 10% PRESENTATION (SHOULD BE GUARANTEED...)

USING FORMULA `WC * $SECTION/80%`

- INTRODUCTION AND LITERATURE REVIEW: 3000 TO 4500 WORDS
- EXPERIMENTAL DESIGN: 2250 TO 3375
- RESULTS AND DISCUSSION: 5250 TO 7875
- CONCLUSION AND FUTURE WORK: 1500 TO 2250

2 Abstract

The CubeSat is a type of small satellite, initially conceived reduce the cost access to space to universities due to its small and standardised 10 cm × 10 cm × 10 cm cubic form factor. The total number of CubeSats launched into space is growing exponentially due to their low cost, doubling every 2.5 y, however the mission success rate has not increased significantly since 2018, levelling off at 75% [1], [2].

Vibration and shock tests are industry standard procedures which aim to emulate launch conditions, however they cannot perfectly replicate them [3]. Testing of CubeSats on suborbital high-power rockets (HPR) is a novel qualification method that can potentially replicate launch conditions more accurately than traditional shaker table tests, and therefore better detect issues and improve the likelihood of mission success. While there have been tests of university CubeSats on high-power rockets [4], there are no direct comparisons to shaker table tests to evaluate their effectiveness as a qualification method.

This paper outlines the construction of a data acquisition system to obtain acceleration data from the HPR launch, the HPR launch and vibration table tests and finally makes a direct comparison of the vibration environment on the HPR launch and vibration table.

3 Acknowledgements

I'd like to thank all the people and organisations who have supported me throughout this project. Dilusha Silva for being a wonderful mentor and for coordinating the project. Michal Zawierta for his expertise flying drones for the drone tests of the CubeSat. Jamir Khan for being a wonderful friend and engineer who worked on the mechanical side of this project, including construction of the high-power rocket, and for putting up with all my delays. Timothy Ludovico for designing the camera payload and being all around wonderful to work with. Jeremy Marelich and AVI for providing their shaker table facilities and conducting the tests. UWA Aerospace for being a wonderful institution who has been with me from first year through my growth as an engineer and has supported me through this project. Space Angel for creating this project and providing expertise and connections to the Indian Institute of Space Science and Technology (IIST). Dr. Priyadarshnam Hari and the Indian Institute of Space Science and Technology for providing their launch expertise and opportunity to launch on POEM. International Space Centre for supporting this project with funding.

Contents

4 List of figures

5 List of tables

6 Introduction

6.1 Background

The University of Western Australia (UWA) Microelectronics Research Group (MRG) is developing a 2U CubeSat to measure the health of vegetation through an infrared camera array [5]. The CubeSat is a type of small satellite designed to reduce the cost of access to space for universities and space startups due to its small and standardised $10\,\text{cm} \times 10\,\text{cm} \times 10\,\text{cm}$ cube form factor. This CubeSat will launch on an Indian Polar Satellite Launch Vehicle (PSLV) in the PSLV Orbital Experiment module (POEM), which will host multiple CubeSats in orbit and will provide services including power and communications to the CubeSat.

The total number of CubeSats launched into space is growing exponentially due to their low cost, doubling every 2.5 y, however the mission success rate has not increased significantly since 2018, levelling off at 75% [1], [2], which implies a need for novel qualification methods. For most single-launch satellites, increased testing is the optimal strategy to minimise failure [2]. Qualification of the CubeSat is required to maximise mission success and is required by the launch provider to minimise the risk of damage to the launch vehicle or other payloads. The MRG is planning to qualify this CubeSat on a suborbital high-power rocket (HPR) in combination with traditional vibration and shock tests on a single degree of freedom (SDOF) electrodynamic shaker table.

Vibration and shock testing are typical tests for CubeSats which are intended to replicate the conditions of launch [1]. Despite their widespread use, SDOF vibration and shock tests do not perfectly replicate the conditions at launch as [3], [6]:

1. The peak flight responses are not able to be achieved since a vibration table cannot simulate steady-state thrust forces since they only can simulate dynamic forces [3].

2. A SDOF test can only excite one axis at a time which is not representative of the launch environment [3], [6].

3. A vibration table tests a "fixed-base" case which has different modes compared to the case where the satellite is fixed to the launch vehicle [3].

A HPR has a higher total impulse than model rockets but a lower impulse than sounding rockets, with a range of 36 N s up to 163 840 N s, and have a sub-orbital trajectory unlike COTS launch vehicles [7]. Suborbital rockets have been used for testing several CubeSats [8], [9], however this qualification method is not in widespread use in the industry.

6.2 Problem identification

For institutions with limited budget, shock and random vibration tests using a SDOF vibration table is the current state of the art (SOTA) method for qualification. HPRs are a potential qualification method which can complement SDOF vibration tests, however there is no prior studies comparing both HPRs and SDOF vibration tests against the

qualification level set by the launch provider. If HPRs can produce a vibration environment similar to the qualification level, HPRs may be a useful complement to SDOF vibration tests and may be useful in increasing mission success rates.

Since HPRs have not been frequently used as a test platform, another issue is the lack of tooling for making HPRs an effective test platform. This research will involve design and evaluation of a combined test and data acquisition platform which:

1. Measures the vibration response of the rocket on the CubeSat required for evaluating the HPR platform and

2. Provides the same power and communications services as the POEM to ensure the payload-under-test has access to the same environment as on launch.

7 Literature Review

This literature review will cover the current testing methods used in CubeSats, the use of suborbital rockets as a qualification method and cover the types of sensors and systems required to record these tests.

7.1 Standard satellite qualification methods

Satellites undergo a panel of qualification tests to maximise the chance of mission success, and may be required by the launch provider to demonstrate that there is minimal risk of the satellite to the launch vehicle and other payloads which may be present. There are multiple satellite qualification standards, an example is the NASA General Environmental Verification Specification (GEVS) which is a panel of tests including electromagnetic compatibility (EMC), thermal, acoustic and vibration tests that are required for all NASA Goddard Space Flight Center projects [10]. Other standards include ISO-15864, JERG-2-002, NASA-STD-7002A, ECSS-E-ST-10-03C and SMC-S-01 [11]. While these standards have flight heritage, being used on many successful payloads, they were designed for medium or large satellites, and therefore fully complying with these standards are out of the budget of most university CubeSat programs [11]. While is no widely used test standard for CubeSats currently in use, since most CubeSat projects perform the minimum panel of tests required by the launch provider to minimise cost, there is a de facto minimum series of tests which are random vibration, shock and thermal vacuum testing [1].

7.2 Vibration

Vibrations are experienced by satellites during transportation and loading, and most prominently during launch [12]. The purpose of vibration testing is to ensure that the satellite will survive transportation and launch conditions, and to find workmanship errors [3], [12].

7.2.1 Welch's method and power spectral density (PSD)

7.2.2 Random vibration / sine sweep vibration test

In the random vibration test, a uniform vibration spectrum is applied to the satellite which tests all the resonant frequencies of the satellite [13]. This range includes frequencies on the magnitude of 100 Hz, since higher frequencies couple to the satellite through acoustic means rather than through the structure [3]. A sine sweep vibration test is similar, but instead of the frequency being randomly sampled it is swept through sequentially from either low to high frequency or vice versa. An example of a random vibration test is shown in figure 1, where frequencies up to 100 Hz were evaluated, and higher frequencies above 100 Hz were attenuated proportional to frequency.

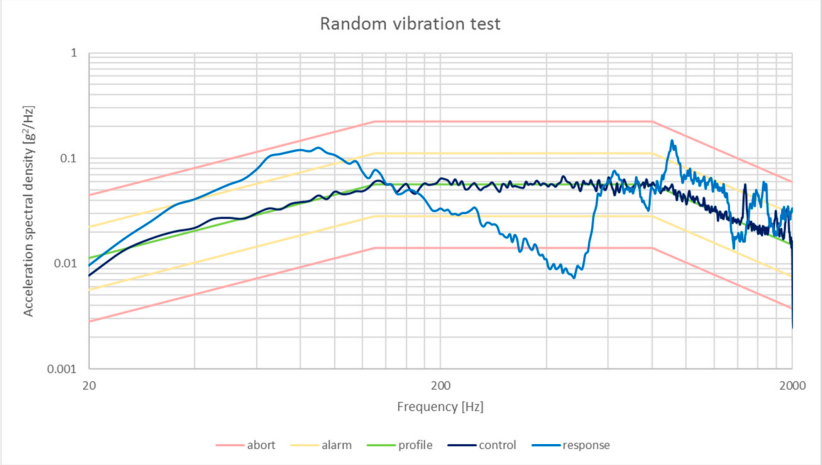

Figure 1: Random vibration test [13]

The limitations of random vibration tests is that the shaker and table will have different modes than the launch vehicle and payload mount, resulting in the test response not perfectly matching the flight response [3], [14]. Gordon and Kern argue that this difference is not a factor in practice since shaker tests are "not intended to be a strength test" [3, p. 7] and that components "should have been strength qualified prior to integration" [3, p. 7]. Component level is argued as a best practice in the CubeSat community [15], however some argue that component level testing is not suited to the short timeline of university CubeSat projects and that more effort should be put into integration testing [16]. If a testing program focuses on integration testing, then this mismatch between shaker table and flight response could result in the CubeSat not being properly qualified.

Finally, although 6 degrees of freedom (DOF) vibration tables exist which can replicate the vibrations experienced in all dimensions during launch, most satellites are still tested with single-axis or random input shakers which only provide one dimension [3], [6], [14]. While Gordon and Kern [3] state that these limitations are adequately managed by testing in all three orthogonal axes separately, Aglietti and Nath [6] created a model

of three, two and single axis vibration tests and found that to match the 3 DOF response with a single DOF table, the satellite needed to be subjected to 2.5 times the g_{rms} forces than in 3 DOF testing, leading to the satellite being over designed [6].

7.2.3 Quasi-static acceleration test (QAT)

A quasi-static test replicates the liftoff stage of flight, where there is a combination of random vibration from engines and quasi-static axial acceleration from the engine and other external forces on the launch vehicle [12], [13], which are approximated as constant forces at selected frequencies as shown in figure 2. The QAT is usually compared to results from coupled loads analysis, where all forces are assumed to be applied to the satellite through the launch vehicle as shown in figure 3 [17].

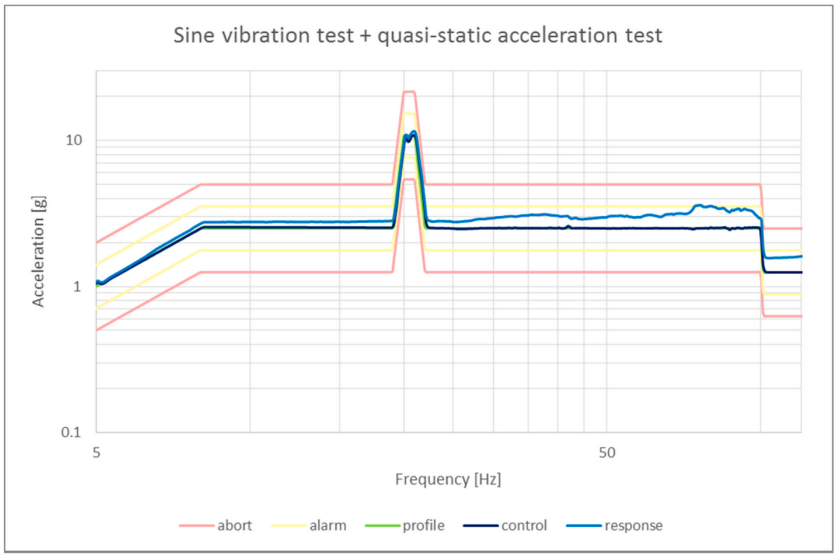

Figure 2: Quasi-static acceleration test. The input profile high acceleration from 20 Hz to 21 Hz, resulting in the response having a force of 10.8 g acceleration around this frequency [13]

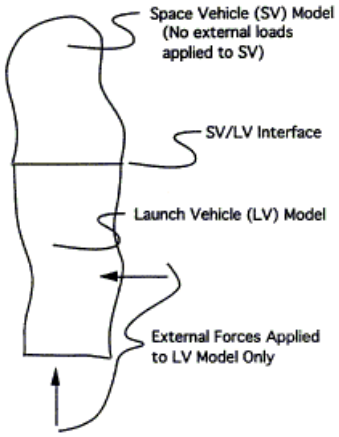

Figure 3: Coupled loads model [17]

The first limitation of a quasi-static acceleration test is that the shaker table cannot apply the peak response evenly on the CubeSat that is predicted by coupled loads analysis (CLA) [3]. Again, Gordon and Kern state that these limitations are addressed by component-level strength qualification. They also state that applying the peak response evenly is not necessary, since if an item does not fail, the correctly applying the response evenly does not greatly increase its likelihood of failing [3]. The second limitation is there is a difference in modes, since a quasi-static acceleration test also contains random vibrations [3].

7.3 Vibroacoustic testing

As stated, low frequency vibrations from 0 Hz to 100 Hz tend to couple well through the payload mount, however high frequency vibrations above 100 Hz are more efficiently imparted on the satellite acoustically [3]. These acoustic loads have an effect on payload electronics [18], and primarily originate from the highly turbulent engine exhaust [18].

Vibroacoustic testing is not necessary for CubeSats due to their small surface area [10], since the magnitude of the acoustic response is proportional to the satellite's surface area to mass ratio [12], therefore the effect of the acoustic loads is negligible. Instead, vibroacoustic testing is more relevant for large and light payloads such as solar panel arrays [12], therefore it will not be part of this research.

7.4 Shock

Shock is experienced by satellites when pyrotechnics are detonated or deflagrated during events such as staging and ignition, the response appears as a range of decaying sinusoids in the 100 Hz to 10 kHz frequency range [12], which decay in 5 ms to 15 ms [12]. The spectrum extends up to 40 kHz, however for analysis frequencies above 10 kHz are assumed to be non-damaging [19], [20]. Pyroshock may cause peak accelerations of up

to 10000 g [20]. High explosives are primarily used for explosive elements on rockets in combination with some low explosives for initiators [19].

Shock is tested using a shock-generating device which is applied to the satellite along all three axes [10], [20], the shock generating device for a CubeSat can be an electrodynamic shaker table [13] with a half-sine, pulse profile [13]. The shock test has similar limitations as the random vibration test, since it also uses a vibration table to affect the satellite.

Shock tests are compared using the shock response spectrum (SRS), which plots the maximum acceleration per frequency bin. The SRS contains an octave slope which rises to the first resonant frequency called the "knee frequency". The octave slope can be approximately 9 dB/octave to 12 dB/octave depending on distance to the source.

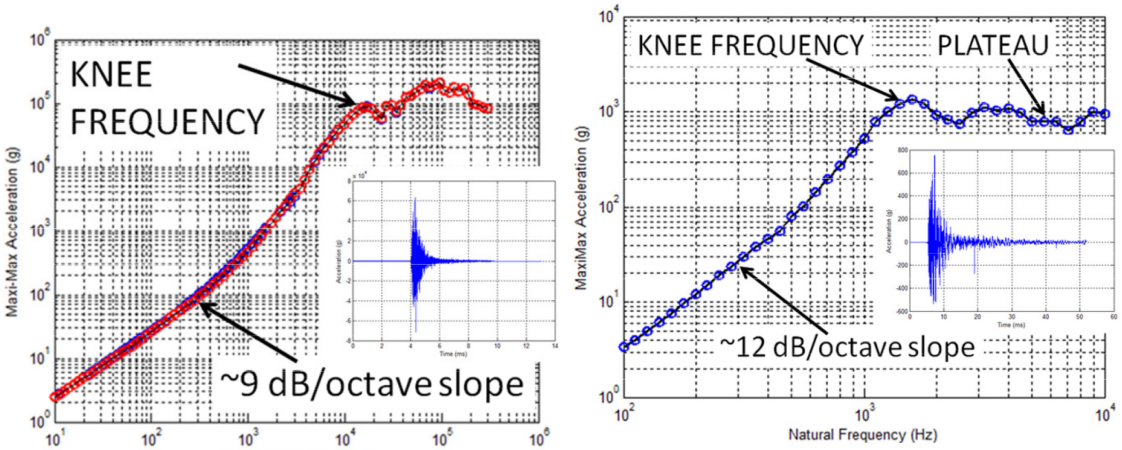

Figure 4: Shock response spectrum of and time-domain shock response. Left: near-field (close to shock source). Right: far-field (distant from shock source) [20]

7.5 Rocket testing of CubeSats

7.5.1 Sounding rockets

Sounding rockets are a class of suborbital rocket used between 40 km and 200 km, above where weather balloons operate [21]. While sounding rockets have been used to launch many CubeSats as the primary launch vehicle for suborbital CubeSat missions, such as in the REXUS-25 mission [22], there has been only one published instance of sounding rockets being used as an additional qualification platform for a CubeSat [4]. The FloripaSat-I CubeSat was tested on a VSB-30 sounding rocket [4] to qualify the CubeSat under launch conditions. This qualification method was intended not to replace, but to complement standard vibration and shock qualification methods [4]. The test measured these launch conditions through the MPU6050 6 DOF inertial measurement unit (IMU) [4].

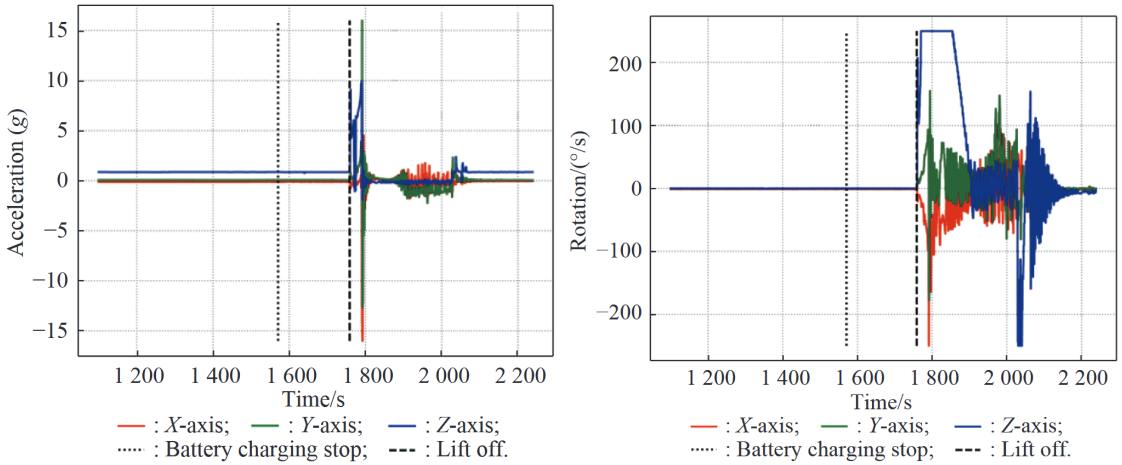

Figure 5: Acceleration in time domain (Left), Angular velocity in time domain (Right) during the launch of FloripaSat-I [8]

While this study does show the time-domain accelerometer and gyroscope measurements from the sounding rocket launch in figure 5, it does not compare the data to other qualification tests in the FloripaSat-I campaign, such as traditional vibration and shock testing. Additionally, the launch data was not presented in the frequency domain through the boost and coast phases of the flight, meaning they could not be compared to the acceleration spectra which was shown for the shaker table testing in figure **??**.

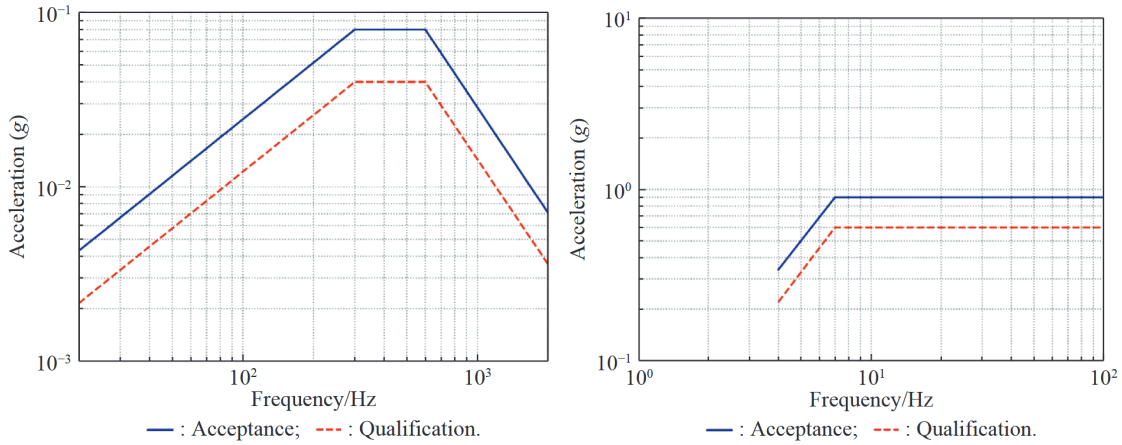

Figure 6: Random vibration (Left) and sine sweep (Right) tests on a shaker table during the qualification of FloripaSat-I [8]

Another shortcoming of the study is that a shock test using a half-sine pulse was not performed. The use of a sounding rocket is a potential method of qualifying the CubeSat's ability to tolerate shocks since there will be shock events when pyrotechnics

are lit to stage the rocket, although the forces will have intensity than on a larger launch vehicle.

7.5.2 High-power rockets (HPR)

While sounding rockets have a significantly lower cost compared to an orbital-class launch vehicle, they cost $1 million USD per launch to launch 200 kg on average **jurist2009COTS**, resulting in a specific cost of $5000 USD/kg, which is still a large amount for university CubeSat programs. High-power rockets (HPR) are a lower-performance but cheaper alternative to sounding rockets, which can leverage the design expertise of university rocketry teams while having similar qualification potential as sounding rockets. A single stage level 3 certification rocket can reach altitudes above 10 000 ft [23] for a cost of only $1200 USD [23]. Despite the potential cost benefits, there have not been any published instances of a HPR being used to qualify a CubeSat.

The typical phases of a HPR launch are

- Boost phase: The HPR is being powered by a solid rocket motor. In most HPR launches, this phase only lasts several seconds at maximum.
- Coast phase: After the rocket motor burns out and produces no thrust the rocket coasts up on a ballistic trajectory to the maximum altitude (the apogee).
- Apogee: This is the maximum altitude the rocket will reach. At this point the drogue parachute is deployed, which limits the rocket's descent velocity to a reasonable rate
- Main parachute deployment: At a fixed altitude above ground level the main parachute is deployed. This parachute has a higher surface area than the drogue chute and slows the rocket down to a safe landing velocity. A main parachute should not be deployed at apogee since this would result in the rocket drifting further which complicates recovery efforts.
- Landing: The rocket lands on the ground and is recovered by the rocketry team for safing (disarming of live energetics) and transportation. While the landing occurs minutes after launch, finding the rocket is a harder task and may occur hours after landing.

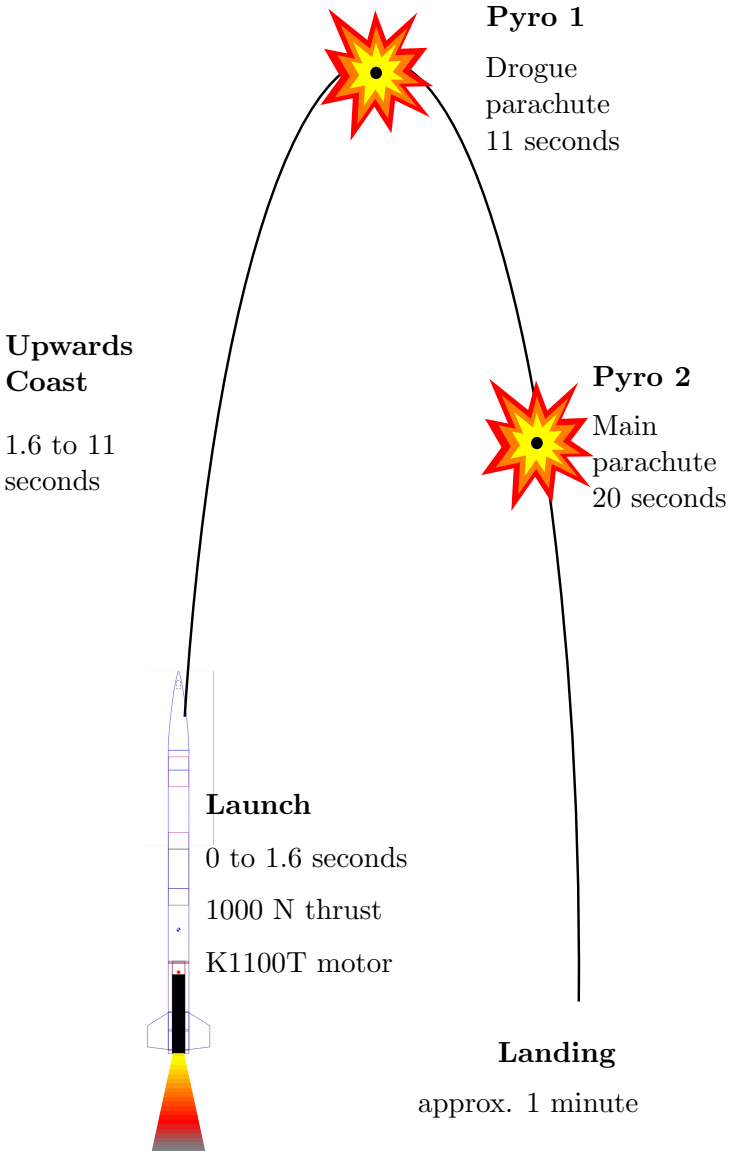

Figure 7: Typical launch of a single stage high-power rocket

One potential issue with HPRs as a qualification platform for shock is that low explosive black powder is used [23] which has different explosive characteristics, such as a subsonic flame front, compared to the high-explosives used in launch vehicles [19] and will therefore produce different shock responses. One study [24] performed finite element analysis of igniters filled with low explosives including aluminium potassium perchlorate and boron potassium nitrate and determined the SRS, shown in figure 8. Compared to the SRS of high-explosives in figure 4, where at a frequency of 1 kHz the acceleration is over 10^2 g [20], in these low explosive simulations the acceleration at 1 kHz is only 10^1 g [24]. Therefore, it is hypothesised that HPRs will not be useful for shock qualification

since the response of low explosives is different from the high explosives used on launch vehicles.

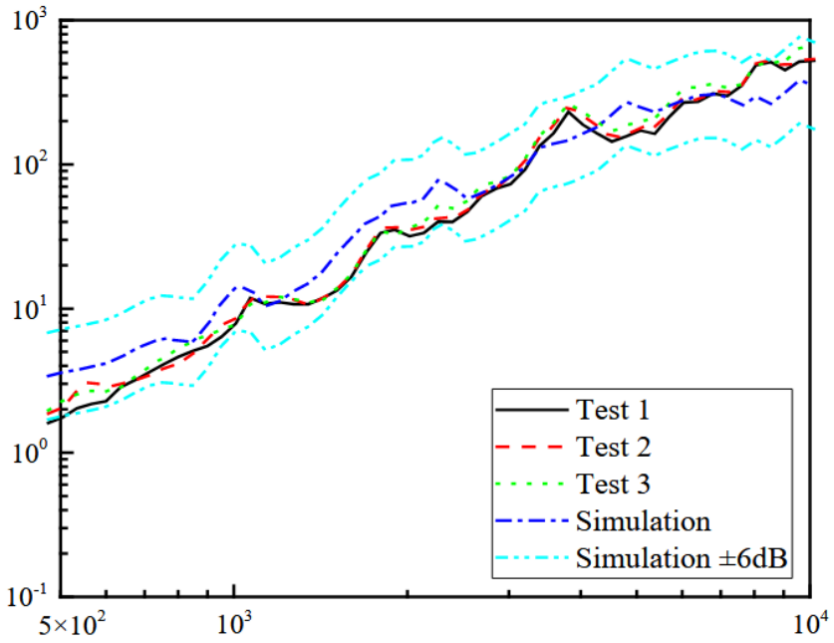

Figure 8: Shock response spectrum from computer modelling of an igniter based on the low explosive aluminium potassium perchlorate [24]

7.6 Avionics systems in high-power rockets

7.6.1 TODO: section

8 Design process

TODO: introduction to design process.

8.1 Design group

The CubeSat design group was made of Peter Tanner, Jamir Khan and Timothy Ludovico. As shown in figure 9, each person is working on a unique part of the CubeSat and requires specific information to be communicated.

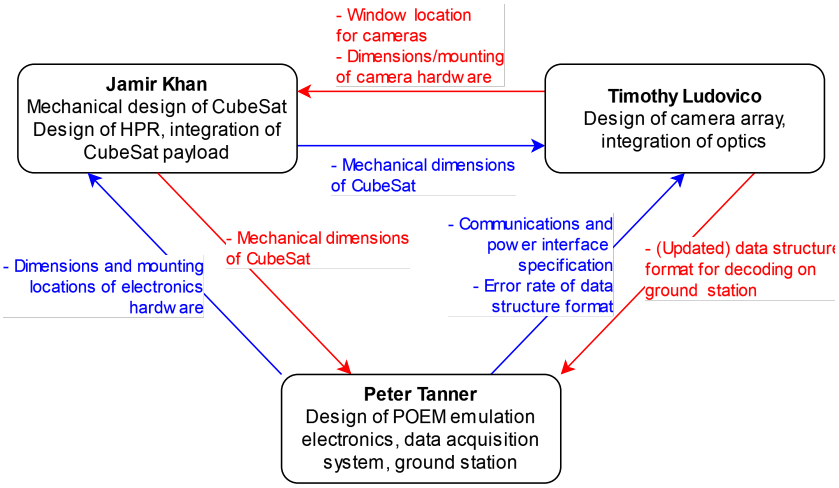

Figure 9: Responsibilities of members on the CubeSat design project and the information required to be communicated between each member.

8.2 Design tools

8.2.1 Altium Designer 24

Altium Designer is an electronics design automation (EDA) tool which is widely used in industry and has been used for design of CubeSat and space hardware [25]. The author chose to use Altium Designer over other EDA tools since they were familiar with this tool having used it in previous projects, which minimises development time.

The design flow in Altium designer is as follows:

Schematic editor A circuit is first implemented using schematic symbol representations of components in the schematic editor. In the schematic view the connections between the components are abstracted using net labels and wires. The schematic view does not necessarily represent the physical layout of the PCB but is intended to convey the connections between components in a format that can easily be read.

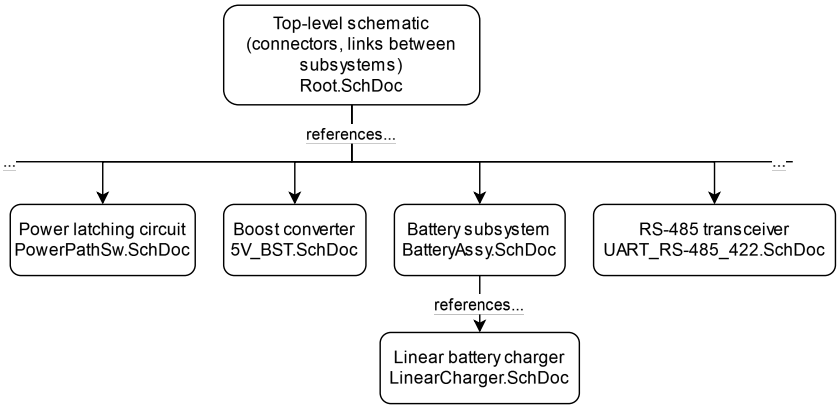

Figure 10: Example of the hierarchical schematic sheet format for the main DAQ PCB.

A root schematic contains references to other schematics which are abstracted as sheet symbols with ports. Each sheet symbol represents a particular subsystem of the DAQ. The hierarchical sheet symbol representation has several benefits, including that it facilitates reuse of designs and allows larger systems to be decomposed into multiple schematics which are easier to modify and read. This is shown in figure 10.

PCB editor Each schematic symbol is a component which links the symbol to a footprint. The footprint is the physical representation of the component and contains information such as

- The land pattern, which is the layout of pads or holes required for mounting the component on the PCB,
- The component's 3d model

The PCB editor contains automated design rule check (DRC) tools which is used in the design process to reduce the likelihood of a faulty PCB. The DRC uses rules set in the project and if a rule is violated, it is reported. This feature is used for example to ensure that microwave-frequency tracks have the correct geometry for impedance matching.

Output jobs Once a PCB is ready to be manufactured, an automated "outjob" ensures that the required design files are automatically generated with the right settings for manufacturing. The files generated include:

- Bill of materials
- Gerber files
- Drill location files
- Pick-and-place component locations

The outjob feature prevents errors such as misconfiguration of output files.

8.2.2 circuit.js

Circuit.js is a simple browser-based analog circuit simulator [26]. Circuits in this simulator can be edited and interacted with in real-time, whereas in traditional SPICE simulators the circuit cannot be edited once the simulation starts. Circuit.js uses a numerical method which is prone to error however, therefore this simulator was used for rapid, real-time prototyping of designs. After these designs were finalised they were simulated in traditional SPICE-based simulators.

8.2.3 LTspice

The simulation of components is done using LTspice, a freeware circuit simulator which uses the SPICE method

LTspice was used to the DC-DC boost converter for this project, which was required to power the internal DAQ systems and the payload. A simulation was performed to characterise the ripple voltage and to validate its performance over a range of input voltages. LTspice has been used for simulation of boost converters in the past and is free which makes it a suitable circuit simulator for this project [27].

Ultimately LTspice was chosen over other freeware SPICE simulators such as PSpice since LTspice contains an "alternate" solver which has less error at the trade-off of simulation time [28]. The reduced error results in the solver converging on a solution, whereas in PSpice or in LTspice normal solver mode it was not able to converge on a solution and the simulation could not be completed.

8.2.4 SolidWorks 2023

SolidWorks is a mechanical CAD software which is used for creating 3d models of the electronics hardware by using the Altium Designer plugin. These 3d models are required for Jamir to complete the mechanical design of the CubeSat and to verify good mounting of the electronic hardware.

8.3 Identification of constraints and requirements

The beginning of the design process involves identification of constraints and requirements.

The ultimate goal of this testing campaign is to receive at least one image from the camera payload from a drone or HPR flight, and launch on the POEM and receive at least one image from orbit. The POEM will remain in low Earth orbit (LEO) for 6 months [29].

8.3.1 Electrical power system (EPC) requirements and constraints

Battery life POEM outputs a consistent amount of power to each CubeSat while on orbit due to its solar panels and battery system, however in the tests it will not be

possible to deploy a solar panel therefore the DAQ system must have adequate battery life to power the camera payload throughout the length of the test.

Voltage and current A requirement of the EPC on the DAQ is to emulate the voltage and current provided by the POEM to one CubeSat to facilitate testing of the camera payload's power electronics. POEM contains a 28 V and 42 V bus, however IIST has informed the design team that a 5 V connection with a maximum current of 1.5 A is provided to CubeSats, with the option to expand to 3 A. The EPC will have to emulate at least one of these power busses.

8.3.2 Environmental requirements

It is possible a future version of this payload will fly with the camera payload on POEM to make a direct comparison between the vibration environment on POEM to the conditions on both a HPR and the shaker table tests. Therefore, the DAQ must go through the same qualification campaign as the camera payload.

Shock, random vibration, sine-sweep test pass The DAQ must remain functional during the vibration environment of the rocket. This means it must pass the IIST recommended qualification procedure, which involves shock, random vibration and sine-sweep tests. These tests are described in more detail in section 9.1.3 Shaker table test.

Cold and hot temperature test pass The DAQ must be able to survive at temperatures of −20 °C to 80 °C as described in section 9.1.1 High-temperature test and section 9.1.2 Low-temperature test. This will influence the components that can be used.

8.3.3 Physical requirements

Physical dimensions The DAQ must have physical dimensions that allow it to fit within the inside space of a 1U CubeSat.

8.3.4 HPR test requirements

GNSS tracking In the original plan, the HPR will launch to a high altitude and may drift away from the launch site. Tracking of the CubeSat will be required to ensure recovery.

Radio link range One of the key requirements stated was receiving one image from a drone or HPR flight. This requires a stable radio link with a protocol that allows the received image to be recognisable even if the link degrades.

8.4 Parts selection and constraints

The first part of the design process is to obtain a list of constraints and requirements for the DAQ system, and from these constraints choose appropriate components to achieve the requirements.

The small payload size and recovery sequence of the HPR presents unique constraints for this data acquisition system, which prevented the use of COTS off the shelf (COTS) DAQs and sensors.

8.4.1 Experimental requirements

This project in addition to design of a DAQ involves design of an experiment to evaluate both HPR launches and shaker tables as comparable qualification platforms to the IIST recommended qualification level.

Sampling rate The accelerometers used must be able to sample at twice the frequency bandwidth of the tests. This is to avoid sampling according to the Nyquist criterion.

Maximum measurable acceleration Pyroshock events and motor launch are high-g events that require accelerometers with measurement scales above these events, otherwise they will saturate at the maximum scale.

8.4.2 Other requirements

2024 Australian Universities Rocket Competition (AURC) regulations This payload was intended to fly on the UWA Aerospace rocket *Svengeance* in the AURC 2024 competition, as part of a collaboration with UWA Aerospace. AURC has additional rules for electronics systems, relevant rules include (but not limited to) [30]:

- Lithium-polymer batteries are not allowed (unless using COTS equipment)
- Connectors must have a positive locking mechanism
- Electronics must be mounted using rigid fixing methods

Budget The cost of the DAQ system must not exceed A$1500.

Time The project must be completed before the end of semester 2 2024 (October 18, 2024)

8.5 Selection of components and basic system design

The constraints in section 8.3 Identification of constraints and requirements will determine the parts that are appropriate for the design. A basic system design was created, since some components depend on how others are configured: for example, using the batteries in parallel requires additional balancing components to be selected in this stage.

Selection of electronic parts must also account for availability at the following suppliers. Parts will not be sourced from other suppliers for reasons including high minimum order quantities or counterfeit components.

1. JLCPCB
2. Mouser
3. DigiKey

JLCPCB is a PCB manufacturing service that will be used to manufacture the PCBs for this project. In addition to manufacturing they provide a service to automatically place and solder components to the PCBs. This component source has advantages over component distributors as they:

- automatically place components, which reduces assembly time and reduces risk of poor soldering compared to manual assembly
- price components at a lower cost that is closer to the wholesale price compared to component distributors

JLCPCB cannot be used for expensive components that need fine control over the amount being purchased, since JLCPCB can only provide component assembly for either two full board or five full boards. Additionally, some components cannot be sourced on JLCPCB. This is the case with the chosen GNSS receiver, which has a very high unit price and should not be assembled on all five boards, and is not available in the JLCPCB catalogue.

Mouser and DigiKey are component distributors which allow the purchasing of individual components, with a higher markup compared to JLCPCB. If a part cannot be purchased from JLCPCB for any reason, it will be purchased from Mouser or DigiKey and manually assembled.

Battery selection COTS 18650 lithium-ion batteries were chosen as the energy source for the DAQ. Advantages of this battery format include:

- The 18650 format encases the battery in a rigid metal cylinder which is well-suited for the space environment [31]. Battery formats which use a flexible pouch, like most lithium-polymer cells, are more prone to outgassing in the vacuum of space [31].
- Compared to other rechargeable battery solutions such as Ni-Cd and Ni-H_2, Li-ion batteries have improved temperature range, energy density and specific energy and cycle life [32].
- COTS Li-ionbatteries are a mature battery format due to widespread use in consumer products [32].

- Extensive flight heritage as they have been proven in other CubeSat missions [31], and are being used on flagship NASA missions, such as Europa Clipper [33].
- Low cost as they are COTS grade and are already produced at scale.

Manufacturers produce a variety of types of Li-ionbatteries with different chemistries, which affect parameters including internal resistance, discharge and charging temperature range and capacity.

The Samsung INR18650-25R Li-ionbattery was chosen for the DAQ platform due to

- Previous flight heritage on CubeSats [34].
- Operation over a large temperature range of $-20\,°C$ to $75\,°C$ and has been proven to be stable at $130\,°C$ [35].
- Good capacity of $2500\,mA\,h$ and high maximum discharge rate of $20\,A$.

Power electronics Power electronics are used to stabilise the battery voltage, since each series Li-ionbattery may have a voltage ranging from $2.5\,V$ to $4.2\,V$ over one discharge cycle.

Two cell configurations were considered for this project:

- 1S3P (one set of 3 batteries in parallel).
- 2S2P (two sets of 2 batteries in parallel, each set connected in series).

Category	**1S**	**2S**
Nominal voltage	$3.6\,V$	$7.2\,V$
Power loss	Higher I^2R losses	Lower I^2R losses
Components required for $5\,V$ output	Boost converter	Buck converter and balancing circuitry
Cost of system	Lower due to lack of balancing	Higher due to balancing circuitry

Table 1: Comparison of 1S and 2S battery packs.

A series battery pack would make sense if the electronics operate on a higher voltage (for example, if there are motors or high-power radios). However, in this application the highest voltage used is $5\,V$ and the I^2R losses between the battery and the power converters is low since they are integrated on the same board. A power system using 2S batteries results in a cost of A$10 for power electronics whereas a 1S system only requires A$2 in power electronics.

Three batteries were placed in parallel to form a 1S3P battery pack, this configuration was chosen as it simplifies the charging circuitry by removing the need for cell balancing circuitry that is required for series battery packs, which reduces cost and simplifies the design. Three cells were selected since this

Item	**Voltage** (V)	**Max unit current** (mA)	**Quantity**	**Max current** (mA)
Payload-under-test	5	3000	1	3000
Pi Zero	5	1300 [36]	1	1200
RFD900x	5	1000 [37]	1	1000
NEO-M9N	3.3	100 + 50 [38]	1	150
LSM6DSOX	3.3	0.55 [39]	2	1.1
ADXL375	3.3	0.145 [40]	2	2.9
SP3485EN	3.3	2 [41]	1	2
XR20M1172	3.3	0.5 [42]	2	1
Total (3.3 V)	-	-	-	157
Total (5 V)	-	-	-	5200

Table 2: Operating voltage and current consumption of devices connected to EPC.

The Texas Instruments TPS61022 boost converter was selected for this 1S system. It has a working voltage range of 1.8 V to 5.5 V which is suitable for a 1S3P Li-ionbattery pack with a working voltage range of 2.5 V to 4.2 V, a maximum output current of over 3 A and can be configured to have an output voltage of 5 V which is ideal for the DAQ and the camera payload [43]. A DC-DC switching converter was selected since it has high efficiency above 90% throughout the input voltage of a standard 1S battery pack [43]. The TPS61022 has an operating temperature range of −40 °C to 150 °C which is adequate for thermal qualification [43].

As the current used by the 3.3 V system is only 0 mA a linear regulator was chosen. This solution results in a small power loss of 0 mW of power loss. An Advanced Monolithic Systems AMS1117-3.3 linear regulator was chosen due to its cheap pricing on JLCPCB of only A$0.20 and since it has been used in past designs with success. It has a high dropout voltage of 1.1 V, which is acceptable for the 5 V input [44]. The AMS1117 has an operating temperature range of −40 °C to 125 °C which is adequate for thermal qualification [44].

Onboard data handling unit (OBDH) The OBDH unit acquires data from sensors and the payload and saves it to a storage device and relays relevant data to the ground station through the radio. The two main requirements of the OBDH is that it has enough resources to be able to process and save the sensor and payload data without losing data, and that it has adequate storage to hold sensor data from one HPR flight.

A first revision of the DAQ used an STM32L476 microcontroller, which had similar peripherals, including UART, I^2C and SPI, however as a microcontroller it does not have an operating system and does not have significant storage. Storage was provided in the form of a 4 GB embedded multimedia card (eMMC) chip, which was chosen since it is directly soldered to the PCB and should be more resistant to vibration than a micro SD card connector.

Due to the issues encountered with the first revision and due to the time constraints,

the second revision uses a Raspberry Pi Zero W v1.3 (referred to as "Pi Zero"). This is a development board which integrates the BCM2835 Broadcom system on chip (SoC), 512 MB of RAM and contains a micro-SD card slot, USB interface and peripherals such as UART, I^2C and SPI [45]. This board was chosen due to its small form-factor compared to larger Raspberry Pis, simplicity of integration compared to the Raspberry Pi compute modules and low cost. The Raspberry Pi platform has been used in low-cost low Earth orbit (LEO) CubeSat applications [46]. It is predicted that in polar orbits that the Pi Zero has a lifespan of 5 years [46], which is adequate for this project since the POEM will cease to maintain its orbit after months. The thermal performance of a Raspberry Pi Zero W is adequate for space applications [46]. While a Raspberry Pi Zero 2W was initially selected, which would have had higher performance compared to the Zero v1.3, it was not possible to acquire one due to supply chain issues.

Typically, a Raspberry Pi runs the Raspbian operating system (OS), which is a Debian fork [45]. Compared to developing for a microcontroller, an OS is easier to develop for as it allows the use of standard Linux utilities for interacting with the system, including `ssh` for remote control, and having each DAQ task in a separate process with separated memory makes debugging easier. This ease of development was required to meet the time constraint of the project.

Due to limitations of the BCM2835 SoC only one hardware UART is available [45], but more are required for receiving data from GNSS receivers. Receiving data through a software implementation of UART is not ideal since it uses a large amount of CPU resources and is prone to missing bits especially on the non realtime OS of the Raspberry Pi which severely limits its usable baud rate. The XR20M1172 dual hardware UART to add more UART ports to the Raspberry Pi through the SPI bus. This UART has a 64-byte first-in first-out (FIFO) buffer and interrupts, which eliminates the need for expensive polling, and has a maximum data rate of $16\,\mathrm{Mbit\,s^{-1}}$, which is more than adequate for GNSS data [42] which has a maximum baud rate of only 38 400 bd. This UART has a temperature range of $-40\,^\circ\mathrm{C}$ to $85\,^\circ\mathrm{C}$, allowing it to survive temperature testing.

Radio downlink The POEM contains a radio downlink which allows experiments to transmit data to the ground at a speed of $5\,\mathrm{kbit\,s^{-1}}$. The radio cannot be used to control the CubeSats from the ground.

The RFD900x radio transceiver was used to emulate this POEM service. This transceiver uses the 915 MHz industrial, scientific and medical (ISM) band and transmits with a maximum power of 1 W using a frequency hopping spread spectrum (FHSS) technique [37]. Data rates from $12\,\mathrm{kbit\,s^{-1}}$ to $224\,\mathrm{kbit\,s^{-1}}$ are available with the default firmware [37]. The RFD900x uses a UART to transmit and receive data [37].

The RFD900x satisfies several constraints. It reduces the time to test since it uses the ISM band, which can be used by anyone provided they follow the Low Interference Potential Devices (LIPD) Class License legislation. The use of the FHSS allows the RFD900x to transmit at the maximum power of 1 W that is allowable by the class license under the frequency hopping transmitters section [47].

Distances of 40 km line-of-sight is possible using the RFD900x [37], which is far greater than the maximum distance achievable with the rocket and drone tests. The maximum drone test scheduled had a altitude of 500 m, and the rocket was intended to fly to 10 000 ft (3 km).

This modem will not be used on the space launch, since POEM will provide a radio downlink, but it must pass environmental testing. The modem has a temperature range of −40 °C to 85 °C, which satisfies the range of temperatures required to pass the temperature testing [37].

Payload communications For the payload communications, a physical layer and data layer need to be specified. The physical layer determines the representation of data as (in this case) electric signals. The data layer determines how data is transmitted and received as frames.

CubeSats use the RS-485 physical layer specification and UART data layer specification to transmit data to POEM. RS-485 was chosen since it is a differential bus which increases immunity to electromagnetic interference from other elements on the launch vehicle, therefore reducing the bit error rate [48]. A combination of RS-485 and UART allows large amounts of data to be transferred since the UART data link specification is simple, especially compared to other protocols such as CAN bus [48].

Since the DAQ needs to emulate POEM services as a constraint, payload communications had to use the combination of RS-485 and UART. The Pi Zero has one hardware UART, this single-ended UART signal needs to be converted to the differential RS-485 signal using an RS-485 transceiver. The SP3485 transceiver was chosen due its low unit cost of A$0.32 and high availability on JLCPCB. The transceiver supports data rates up to 10 Mbit s^{-1}, which is more than adequate for the 5 kbit s^{-1} downlink speed. It uses a 3.3 V logic level on the single-ended side, which is required to interface with the Pi Zero without level shifting [41]. The EN-L variant was chosen due to its extended temperature range of −40 °C to 85 °C required to pass environmental testing [41].

GNSS tracking The DAQ system must be able to track the HPR throughout the full launch to enable recovery as stated in section 8.3.4 HPR test requirements. This will be achieved through a Global Navigation Satellite System (GNSS) receiver, which receives signals from GNSS satellites and determines the position and altitude of the receiver. The u-blox NEO-M9N will be used for tracking [38]. This is a multi-GNSS receiver which is able to receive from multiple GNSS constellations simultaneously, which results in a faster acquisition time and greater interference immunity [38]. The receiver can report position with an accuracy of 2.0 m (circular error probable), which is adequate for a HPR tracking application [38]. The NEO-M9N was used instead of other u-blox receivers due to its high navigation update rate of 25 Hz which is useful due to the high speed of a HPR flight [38].

Since POEM provides the location of the CubeSat and due to the speed and altitude restriction of the NEO-M9N of 500 m s^{-1} and 80 km respectively, this receiver will not be present on the space launch and is only required for the HPR launch.

A differential GNSS (DGNSS) solution was considered and tested based on the u-blox ZED-F9P, however the drone test did not require the centimetre level precision of the ZED-F9P, so it was not used in the final design.

Accelerometers Micro-electromechanical systems (MEMS) based accelerometers were chosen for the DAQ due to their low cost and low power consumption compared to traditional piezoelectric accelerometers. Two accelerometers were chosen, the ADXL375 and LSM6DSOX.

The STMicroelectronics LSM6DSOX is a MEMS inertial measurement unit (IMU) which has a $\pm 16\,g$ accelerometer and $\pm 2000\,\mathrm{m^{\circ}\,s^{-1}}$ gyroscope, both with a sampling rate of 6666 kHz. This accelerometer is used to characterise the random vibration spectrum of launch due to its high sampling rate.

Due to the low full-scale of the LSM6DSOX of only $\pm 16\,g$, the ADXL375 was chosen to characterise the shock response of the payload to pyroshock due to its significantly higher full-scale range of $\pm 200\,g$.

System block diagram A block diagram of the system using the parts chosen is shown in figure 11.

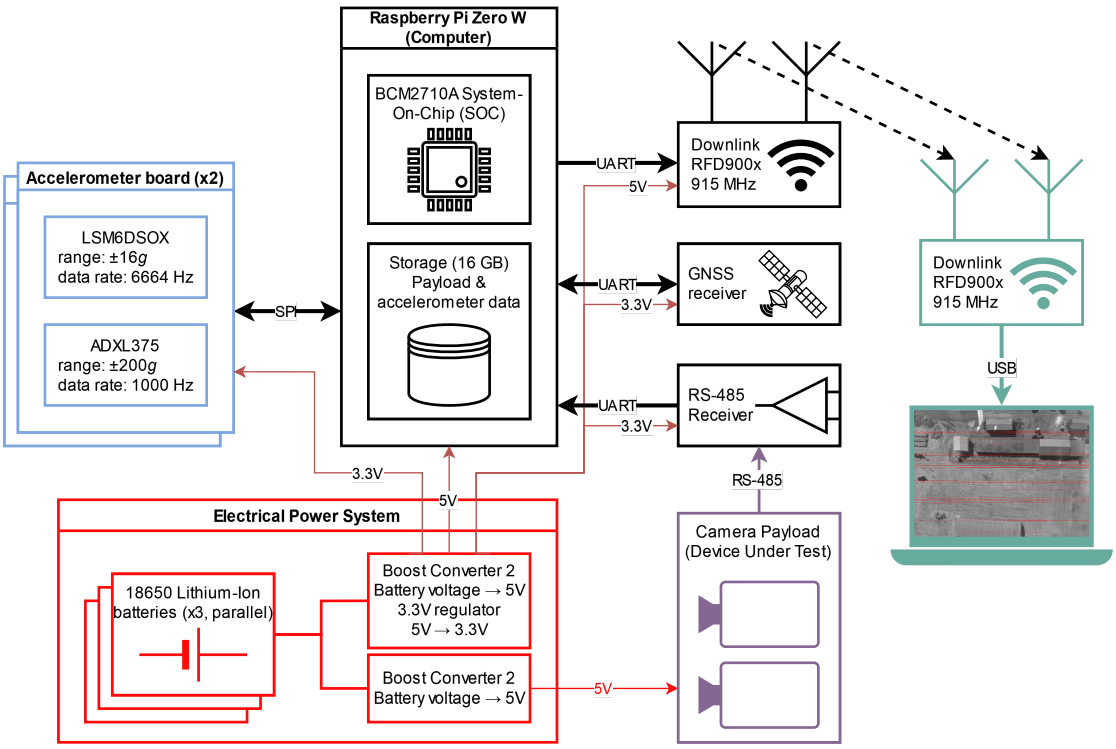

Figure 11: Block diagram of the CubeSat, including connections to the camera payload and ground station over radio downlink.

8.6 Implementation of parts into design

After the components are selected, they are integrated into the design as shown in figure 12.

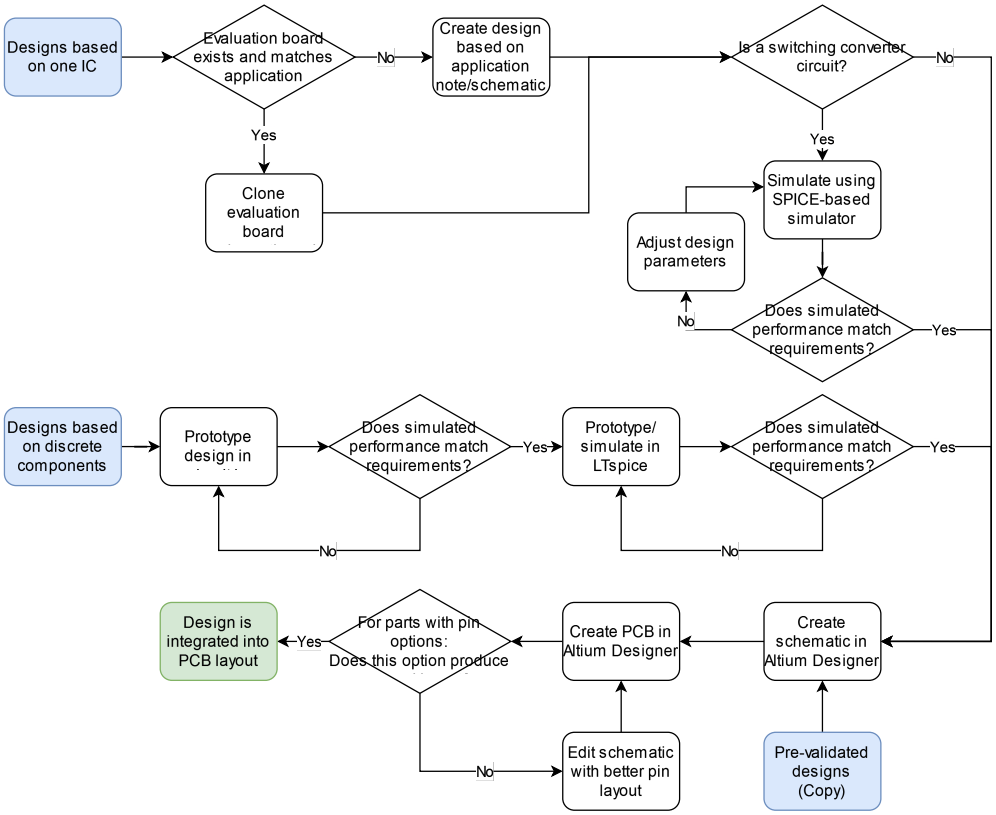

Figure 12: Workflow for integrating a design into a PCB.

Schematic-level There are three cases for integration of subsystems into the DAQ design:

1. Subsystems based around single ICs, for example power converters, are implemented by using the process outlined in the application note or by copying a reference design or evaluation board design if it exactly matches the application in the DAQ. As an additional precaution, switching converters are simulated in a SPICE simulator to ensure the output is stable over the range of input voltages and output currents.

2. Discrete components are used to implement some simple circuits to save on part cost. These are prototyped in circuit.js, then once working in circuit.js are simulated in a SPICE simulator.

3. Some subsystems have already been validated on other projects and are able to be directly applied to the DAQ system, the schematics for these designs are copied into the project.

A subsystem is implemented as a single schematic sheet in an Altium PCB project and connected to other schematics using the hierarchical sheet system. When a subsystem is added, a commit for the project is created and pushed to a central version control system (VCS) server.

PCB setup Before any subsystems are laid out in the PCB, several parameters about the PCB are agreed upon.

Firstly, the physical dimensions of the PCB are negotiated with the rest of the design team to ensure it will fit. After the limits for the PCB dimensions are determined, the size of the PCB is determined according to the function of the board. It was decided to use a PCB size of 80 mm × 80 mm for the DAQ boards since this is the maximum size available for the PCB, and larger PCB areas result in higher gain for the patch antennas to be used for receiving GNSS signals. For the MEMS accelerometers, a PCB of 22 mm × 22 mm was chosen as it is the minimum size possible to fit both accelerometers and mounting holes, and minimising the PCB area maximises the resonant frequency of the accelerometers.

The stackup is then decided, which determines the number of PCB layers and the purpose of each layer. The DAQ uses a standard signal-ground-power-signal stackup since this board contains many components and therefore a dedicated power layer would be useful. The GNSS board contains few components and uses a stackup of full grounds to maximise RF performance. Four layer stackups are used since these are cheap to manufacture at JLCPCB for boards under 100 mm × 100 mm and over 50 mm × 50 mm, and four layers allows simpler routing and improved signal integrity due to being able to dedicate two planes to power and ground. The accelerometer board uses a two-layer signal-signal stackup since there are few components to route and to save cost.

Layer	DAQ	GNSS receiver	Accelerometer
Top layer	Signal	Ground	Signal
Layer 1	Ground	Ground	N/A
Layer 2	Power (3.3 V)	Ground	N/A
Bottom layer	Signal	Ground	Signal

Table 3: Stackup of each PCB

Prior to placing laying out any subsystems, PCB rules are set according to the JLCPCB capabilities page.

PCB-level Once a subsystem is finished, the components are laid out in the PCB using general PCB design rules including:

- Using the manufacturer's sample layout and PCB layout guidelines, if they exist
- Placing the majority of components on one side to allow cheaper PCB component assembly, and placing large or manually soldered components such as connectors on the opposite side
- Minimising track distance
- Using large polygons for power routing
- Placing decoupling capacitors close to the part's VCC pins

Additional PCB rules are created where necessary, such as to enforce the geometry of RF tracks or clearance rules.

Finalisation of design and manufacturing After the PCB design is finished, an automatic design rule check (DRC) is run to find any errors that would affect manufacturing. The manufacturing outjob is run to generate artefacts such as Gerber files, the bill of materials for automated and manual manufacturing, and component locations for pick-and-place. These artefacts are sent to JLCPCB to design and partially assemble the PCBs. The manual manufacturing BOM is used to purchase components from component distributors.

After receiving the boards from JLCPCB, some basic tests are conducted (such as ensuring that voltage domains and ground are not short-circuited). After this, additional components are manually assembled either using hot-air or a soldering iron. After soldering, the manual solder joints are inspected to ensure they are not cold joints, and the boards are again tested for short-circuits.

Software development process The Raspbian OS is flashed on to an SD card with settings to allow the Pi Zero to connect to a local Wi-Fi network. An external computer is used to connect to the Pi's secure shell (`ssh`) server and log into the Pi. After this, the USB Ethernet gadget is configured on the Pi and host computer sides which allows the host computer to `ssh`into Pi without needing a Wi-Fi network, which will be useful for field debugging.

A combination of Python scripts and C programs were used for different parts of the DAQ. Python is used for tasks which do not require many system calls and do not require high optimisation, such as transferring data from the payload to the radio. The advantage of Python for these tasks is speed of development. Some tasks, such as reading data from the accelerometers, require many system calls and has considerable performance impact when using Python. For these tasks, a program is written in C and compiled on the Pi Zero. C has less overhead compared to Python as it is a compiled directly to ARM assembly, whereas Python is interpreted to an intermediate representation which is executed by the Python virtual machine which adds overhead.

A Samba server was set up on the Pi Zero to allow code developed from a PC to be copied over to the Pi, and to allow an integrated development environment on the PC to access libraries and headers present on the Pi Zero.

8.7 Preliminary testing

Several preliminary tests were conducted to test the

- Integration testing with camera system
- Ground distance testing

9 Design evaluation framework

The design evaluation framework will consist of three major types of tests:

- Environmental tests.

  Hot and cold temperature testing.

  Shaker table.

- Vehicle tests.

  Drone.

  Rocket.

- Experimental evaluation.

  Evaluation of accelerometers.

9.1 Environmental testing

If this research continues, the DAQ will need to fly with the CubeSat on the PSLV to obtain vibration data that can be directly compared to the rocket and shaker table tests. Therefore, the DAQ will have to go through the same environmental testing campaign as the camera payload. The objective of these tests is to evaluate the resilience of the DAQ in the environment of space and during launch.

9.1.1 High-temperature test

IIST recommends a qualification test where the CubeSat placed in a thermal vacuum chamber for 2.5 h and is heated to 70 °C. The CubeSat electronics are turned on and tested during the final 30 min of the test.

Due to time restrictions it was only possible to do a preliminary high-temperature test with a consumer oven on only the electronics section of the payload (the combined camera and DAQ assembly).

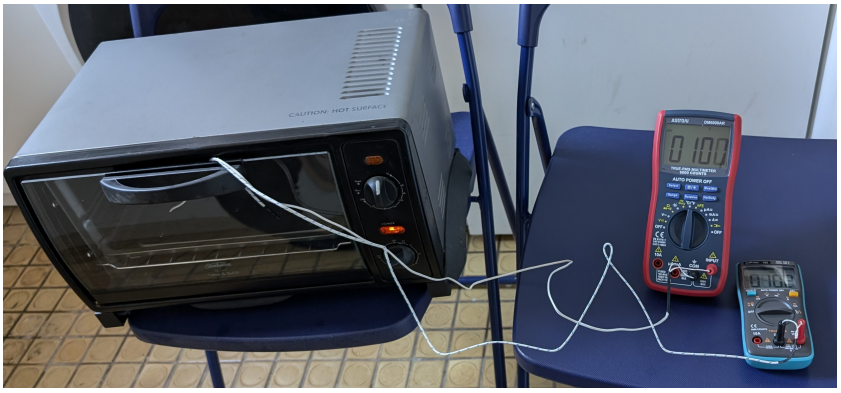

Figure 13: High-temperature testing setup

The DAQ was evaluated based on how much time the connection between the DAQ and ground station is lost.

9.1.2 Low-temperature test

IIST recommends a qualification test where the CubeSat is placed into a thermal vacuum chamber for 2.5 h and is cooled to −20 °C. The CubeSat electronics are turned on and tested during the final 30 min of the test.

Due to time restrictions it was only possible to do a preliminary low-temperature test with a consumer freezer. To prevent condensation from developing on the electronics during the test, which would not occur in the thermal vacuum chamber, the electronics were placed in an airtight bag prior to the test and pressurised with pure nitrogen gas for 5 min to displace air containing moisture.

Frequency (Hz)	**PSD** ($g^2\,\mathrm{Hz}^{-1}$)	g **(RMS)**	**Duration** ($\mathrm{s\,axis}^{-1}$)	**Axis**
20	0.002	13.5	60	Three axes
60	0.002			
250	0.138			
1000	0.138			
2000	0.034			

Table 4: IIST recommended random vibration test profile for qualification of CubeSat for launch on POEM.

Figure 14: Low-temperature testing setup

The DAQ was evaluated based on how much time the connection between the DAQ and ground station is lost.

9.1.3 Shaker table test

IIST recommends that the CubeSat be mechanically qualified using a single-axis electrodynamic shaker table using random vibration, sine-sweep and half-sine shock tests.

Random vibration The IIST recommended qualification level for the random vibration test is specified in table 4.

This random vibration profile is standard in industry, other launches of satellites on the PSLV use similar vibration profiles.

The IIST recommended random vibration test profile was used without modifications in the final shaker table testing.

Sine-sweep The IIST recommended qualification level for the sine-sweep test is specified in table 5.

Longitudinal		Lateral		Sweep Rate	Axis
Frequency	**Level**	**Frequency**	**Level**		
10 Hz to 16 Hz	20 mm DA	10 Hz to 16 Hz	12 mm DA	$4\,\mathrm{oct\,min^{-1}}$	Three axes
16 Hz to 100 Hz	10 g	16 Hz to 100 Hz	6 g	$4\,\mathrm{oct\,min^{-1}}$	Three axes

Table 5: Vibration Data: Longitudinal and Lateral Details with Sweep Rate and Axis Merged

Shock The IIST recommended qualification level for the shock test is specified in table 6.

Amplitude	Duration (ms)	Shock profile	Axis
50 g	10	Half sine	Single-axis shocks, for all three axes

Table 6: IIST recommended shock test profile for qualification of CubeSat for launch on POEM.

9.1.4 Drone test flights

Drone tests were used as a qualification platform for the HPR launch since drone tests:

1. Use the expertise of the UWA Aviation Laboratory, which is participating in the project.
2. Are repeatable, whereas the rocket test can only feasibly be done once per launch season.
3. Have greater control over the position compared to the suborbital rocket launch and will better qualify the machine vision algorithms.

The drone test evaluates the communications between the camera payload and the communications downlink stability in real time. A successful test involves receiving at least one frame from the camera payload at a reasonable quality.

9.1.5 High-power rocket test flight

The high-power rocket (HPR) test flight is used as an experimental qualification method for the CubeSat. This DAQ system is used to evaluate the effectiveness of the HPR flight by using accelerometers, but the HPR flight also serves as a milestone for evaluating the effectiveness of this DAQ for this type of application.

9.2 Evaluation of accelerometers

Typical parameters for the evaluation of accelerometers include TODO:

9.3 Evaluation of downlink

9.4 Evaluation of GNSS tracking

9.5 Evaluation of electrical power system

10 First revision of test and POEM emulation electronics TODO: decide whether to keep or remove.

The POEM provides services such as tracking, telemetry and command (TT&C), electrical power system (EPS) and on-board data handling (OBDH) to the CubeSat, therefore these systems are not integrated into the CubeSat under test and must be provided by a separate system on the HPR which emulates the POEM services. The POEM emulator consists of three PCBs: A combined EPS and OBDH board, a tracking board and a telemetry and command board. This emulation and qualification platform will be referred to as DAQ v1.

10.1 On-board data handling (OBDH)

Two OBDHs are arranged in a dual redundant configuration and are linked to each other via controller area network (CAN) bus. When the hot spare detects that the primary OBDH is outputting bad data or is not responding, the secondary OBDH will take over control of the communications link. This redundancy ensures the likelihood of not obtaining experiment data for this research is minimised. In the best case, this will provide two independent data sources for research. Both OBDHs will still store data to their respective eMMC modules for post-flight analysis.

10.2 Accelerometers

MEMS accelerometers, which will provide the data for this analysis, are located on independent modules and on the OBDH computer. The low-cost LSM6DSO accelerometer will be used due to its low cost and acceleration range of 16-g and bandwidth of up to 6664 Hz [39], which will be used to cover the quasi-static acceleration and random vibration cases. As shown in figures 1 and 2, the g-levels and bandwidth are relatively low and are met by the LSM6DSO.

The independent accelerometer modules will contain a microcontroller, regulator and accelerometer in a small package which can be mounted at various points on the CubeSat, to measure how evenly the response is applied to the CubeSat. The microcontroller will compress the accelerometer data and send it to the OBDH over CAN bus. The OBDH will generate a clock synchronisation signal to ensure the accelerometer measurements are synchronised. The modules will be attached to the CubeSat using adhesives due to its acceptable performance at the frequencies being measured, and ease of use compared to screws.

Measuring the shock response is significantly more difficult due to the high acceleration levels and the large bandwidth [20], which are not well-suited for low-cost MEMS

accelerometers. Instead of measuring the full spectrum, the slope will be measured and compared using the low-cost ADXL373 accelerometer which can measure up to 400-g at 2.56 kHz, which is enough to characterise the slope, which is the only parameter required to show that a rocket is inadequate for qualifying shock.

10.3 Electrical power system (EPS)

A 2S lithium-ion battery pack and two 5V boost converters will be used to power CubeSat and the emulator. Two independent EPS will be connected in an OR-ing configuration so that if one fails, the other will provide power. The CubeSat and emulator will have separate boost converters, and the power to the CubeSat is capable of delivering the full 5V @ 3A which is the specified amount of power available to the CubeSat on the POEM.

10.4 Telemetry and command

An RFD900x radio will be used to downlink the data from the CubeSat and the engineering sensors. This link is optimised for relatively high speed and to have the full 300 kbps capacity that the POEM can provide to the CubeSat. The experiment data required for this research will be downlinked as part of the engineering data, to ensure that data is available to continue research in case the rocket crashes and the onboard memory is destroyed.

The tracking and command system will be on a separate low-bandwidth LoRa radio which is optimised for high link budget and reliability.

10.5 GNSS Tracking

The GNSS tracking board contains a standard precision NEO-M9N GNSS receiver and the ZED-F9P differential GNSS (DGNSS) receiver. A NEO-M9N was selected against other standard GNSS receivers due to its high maximum position, velocity and time (PVT) update rate of 25 Hz. The main purpose of the NEO-M9N is to serve as a simple backup GNSS receiver for reliable tracking purposes, since it does not require an RTK data stream.

The ZED-F9P differential receiver has centimetre-level accuracy and will enable the heading of the rocket to be accurately determined, which is required for this research since the heading may change throughout the flight and this will need to be accounted for when analysing the data since there are 6 DOF, instead of just one in traditional shaker table tests.

10.6 Drone testing

Prior to flight on a HPR the DAQ v1 was tested on a drone. TODO:

-

10.7 Results

One of the objectives of this research is to design a platform for qualification of CubeSats. The first revision of the qualification platform was not used in the final design due to several issues:

- The STM32L476 did not have enough resources to move data from the sensors and camera payload to the payload at an adequate speed. A benchmark using CrystalDiskMark, in figure 8 shows that the maximum throughput is $0.84\,\mathrm{MB\,s^{-1}}$, and while only 60% of the throughput is being used as shown in **??**, between reading from the data sources and writing to the storage there is not enough resources in practice to do this at an adequate speed, resulting in the maximum sampling rate of the sensors to be limited.
- Due to space limitations on the rocket, it was not possible to have two redundant systems. The next revision would use only one DAQ.
- By the end of this section, it was understood that centimetre level positioning was not required to obtain good results from the camera system.
- At the end of this revision it was concluded that the STM32 platform was not flexible enough to complete the research objectives in time.

Data source	Data rate	Notes
LSM6DSOX	$0.41\,\mathrm{MB\,s^{-1}}$	16 byte structs are generated at 6664 Hz for both acceleration and gyroscope data for two sensors.
ADXL375	$0.038\,\mathrm{MB\,s^{-1}}$	20 byte structs generated at 1 kHz for two sensors.
Camera	$0.054\,\mathrm{MB\,s^{-1}}$	460 800 bd
TOTAL	$0.502\,\mathrm{MB\,s^{-1}}$	60% of maximum sequential write bandwidth.

Table 7: Data sources and their data rates.

Test	Read [MB/s]	Write [MB/s]
SEQ1M Q1T1 (1 task, 1 thread)	0.84	0.84
RND4K Q1T1 (1 task, 1 thread)	0.75	0.66

Table 8: CrystalDiskMark benchmark of DAQ v1.

11 Final design of DAQ system

11.1 Power electronics

Subsystem design and simulation The TPS61022 boost converter is used in the final design to convert the battery voltage to a stable 5 V output. The datasheet contains

a reference design (Figure 8-1) which is specified for an input voltage of 2.7 V to 4.35 V, output voltage of 5 V and output current of 3 A, which matches the operating conditions of this subsystem [43].

The inductor selected for the converter subsystem is the ASPI-0630HI-1R0M-T15, which is a 1 µH coil with a low DC resistance of 10 mΩ. The coil has a saturation current of 20.5 A which is above the 8 A maximum switching current. To make manufacturing simpler, the voltage divider was changed from $R_1 = 732\,\text{k}\Omega$ and $R_2 = 100\,\text{k}\Omega$ to use $R_1 = 750\,\text{k}\Omega$ and $R_2 = 100\,\text{k}\Omega + 2\,\text{k}\Omega$ since these resistor values are available on JLCPCB. A 1 pF compensation capacitor was also added. To evaluate the effects of these choices, the converter was simulated in LTspice with a single fully charged lithium-ion battery as the input.

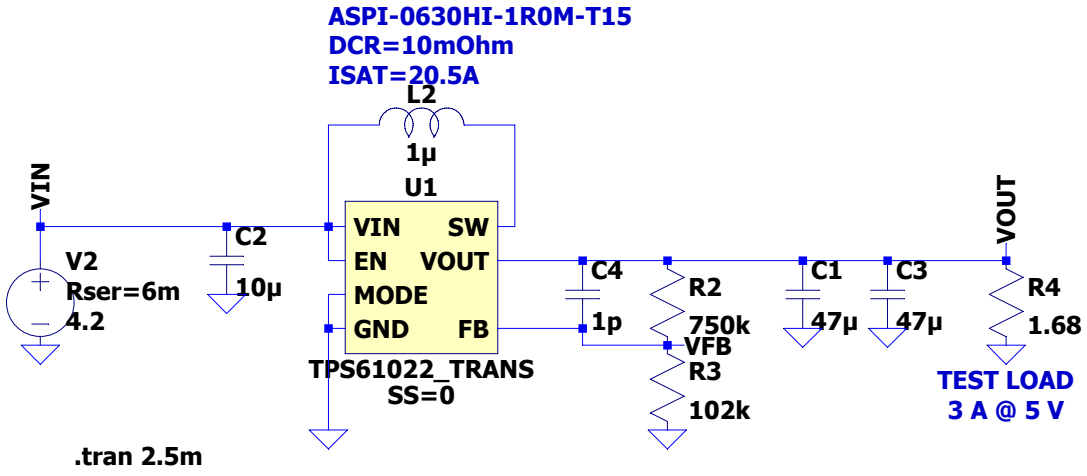

Figure 16: LTspice schematic representation of TPS61022.

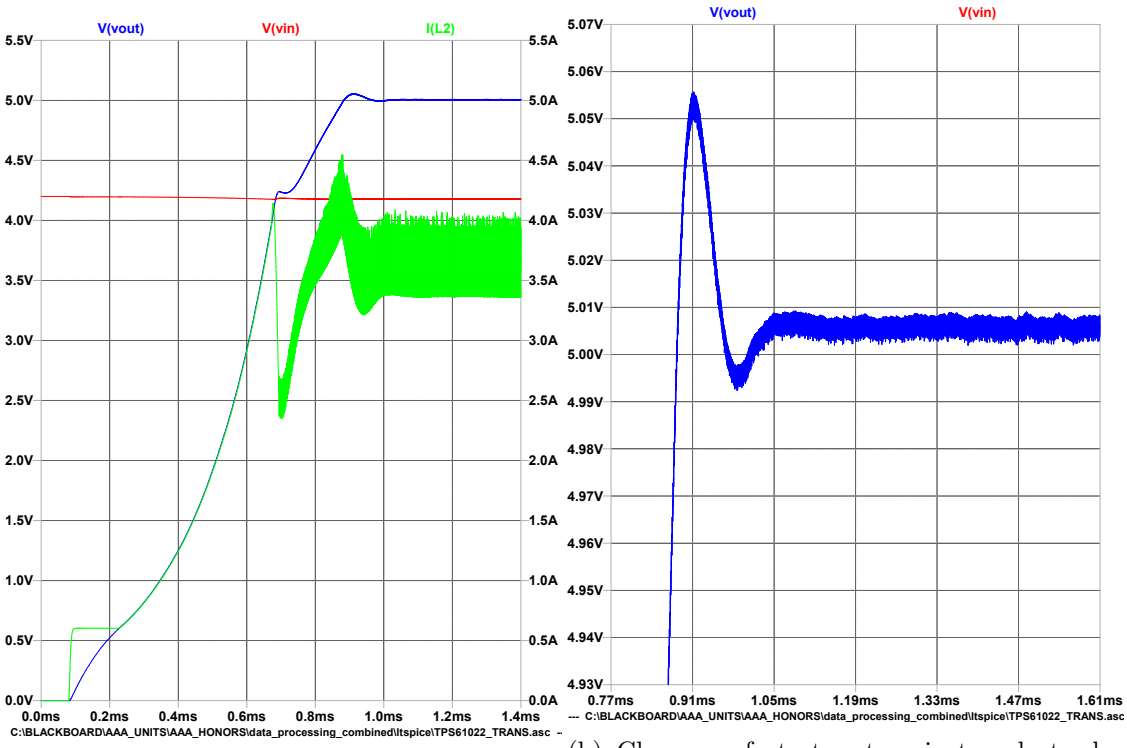

(a) Startup and steady-state behaviour.

(b) Close-up of startup transient and steady-state behaviour.

Figure 17: Simulation of the TPS61022 in LTspice using component values close to the datasheet as shown in figure 16.)

As shown in figure 17, during startup there is a small voltage overshoot of 0.06 V but this is negligible and well within the tolerance of the components. The steady-state output voltage has a mean of 5.006 V and a peak to peak ripple voltage of 7 mV, or a ripple of 0.15%, which is more than adequate for this application since it is mainly digital logic.

The simulation also shows that the power system will work up to 3 A, which is the output current required to emulate the power capabilities of POEM. Two TPS61022 boost converters will be used in the final design: one will be dedicated for the payload-under-test, and the other will power the DAQ system. This allows the payload to be able to receive the maximum current able to be provided by POEM, and also isolates failures in either system from affecting the other.

The 1S3P battery pack was mounted on the reverse side of the PCB due to the amount of space it consumes, as shown in figure **??**.

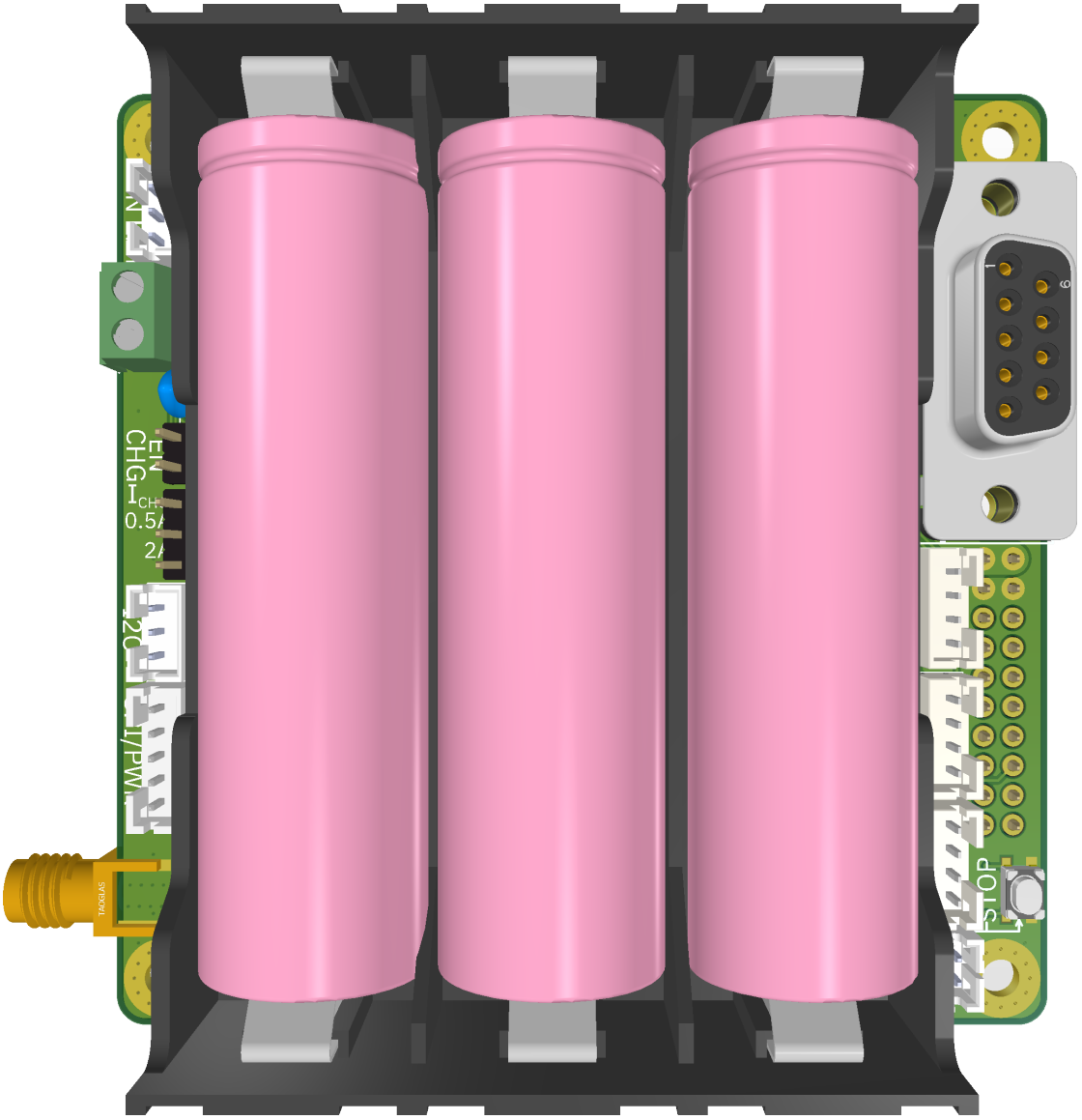

Figure 18: Battery mounting on reverse side of DAQ PCB.

The battery pack can be charged by connecting 5 V power to a charging terminal block. Two 1 A TP4056 linear Li-ionbattery chargers were connected in parallel to the battery pack to allow a maximum charging current of 2 A.

Integration into DAQ system A single schematic was created for the TPS61022 based off the successful LTspice simulation and instantiated twice in the root schematic. A PCB layout based on Figure 10-1 from the datasheet was used and is shown in figure 19 [43].

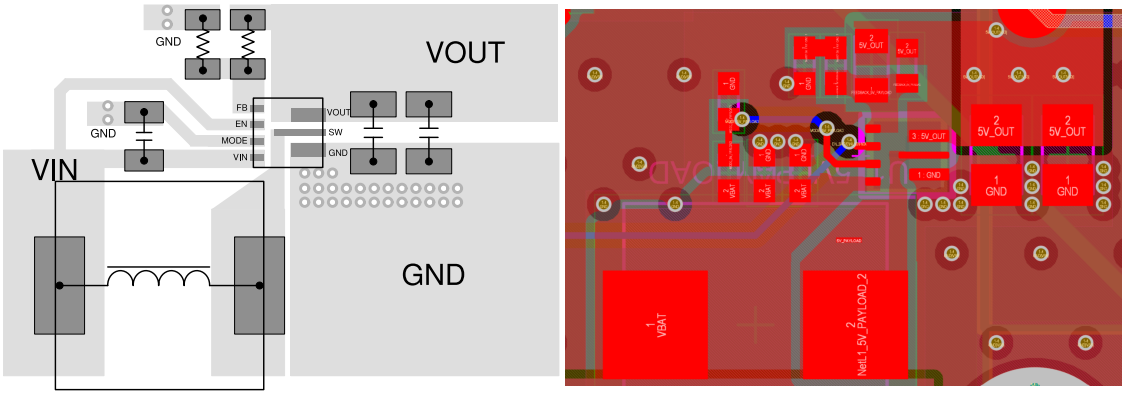

(a) Reference PCB layout [43].

(b) PCB layout implemented in DAQ system.

Figure 19: Simulation of the TPS61022 in LTspice using component values close to the datasheet as shown in figure 16.

A schematic was also created for the TP4056 linear charger, and instantiated twice.

11.2 Camera communications interface and camera data downlink

Connector The final design of the camera payload interface uses a DE-9 connector. This was chosen due to its low cost and ability to be secured using bolts instead of by friction alone. The pinout of the connector is shown in figure **??**. The RS-485, power and ground lines are duplicated for redundancy.

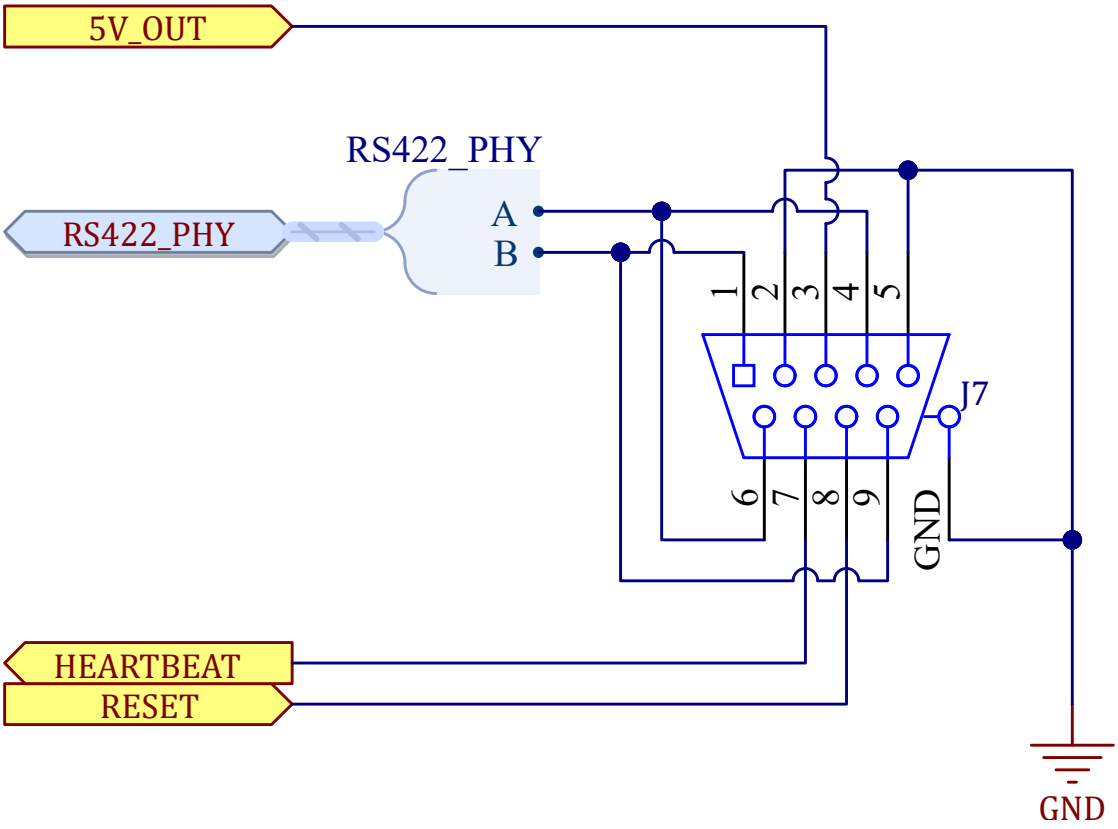

Figure 20: Pinout of DE-9 connector.

A female DE-9 connector is soldered to the DAQ, a male solder cup DE-9 terminal is soldered to 22 AWG copper cable to form the wire harness to the camera payload.

RS-485 receiver The SP3485EN-L/TR RS-485 transceiver is used to convert the RS-485 signalling to single-ended UART. The transceiver is fixed in receive mode since there is no way for the POEM to send data to the payload. The transceiver contains a 120 Ω d.c. termination as this is the end of the RS-485 bus, the resistor is sized to handle the power dissipation of a 5 V RS-485 bus. The receiver contains a PSM712-LF-T7 transient voltage suppressor (TVS) diode array, which is designed to prevent the transceiver from being damaged by electrostatic discharge (ESD) due to manual handling of the connector.

Transport layer The camera payload communicates with the DAQ through UART at the transport layer. The settings in table 9 were agreed upon and are used on both the payload and DAQ sides:

Attribute	Value	Note
Speed	57 600 bd	This is significantly more than the 5000 bd connection provided by POEM, but the drone and HPR tests have limited time and require faster transmission to receive any picture during the test.
Data bits	8	
Stop bits	1	
Parity	None	
Flow control	None	This is a one-way connection, so software flow control is not possible.

Table 9: UART settings.

Presentation layer Several simple formats are used in the presentation layer for this project. The data stream may contain either messages or image data.

Messages consist of a header, the message data of a variable length and an end of message marker as shown in figure 21. The header is sufficiently long and unique that it should not appear in the image data stream. Since messages are not often transmitted, this overhead is acceptable.

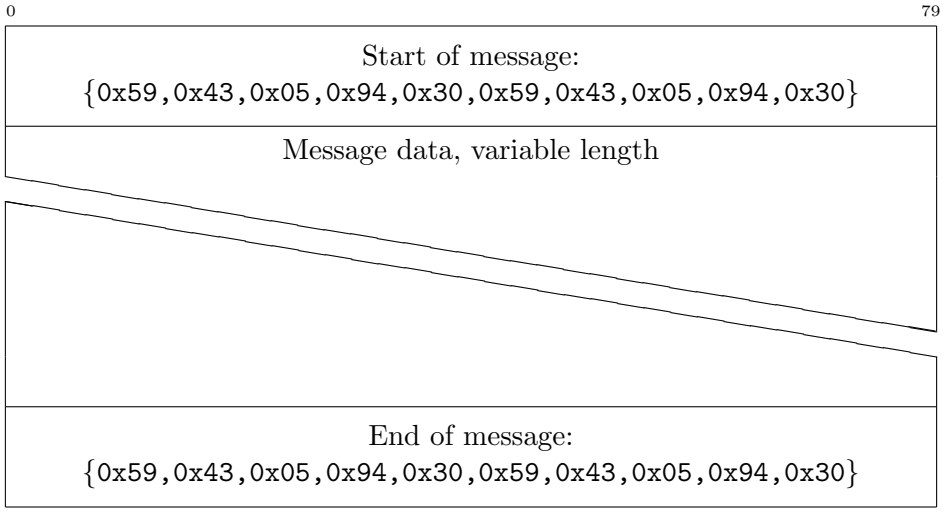

Figure 21: Message structure.

A chunk protocol is used for the transmission of images in the final design. A preliminary design simply sequentially transmitted each byte of the image, which was adequate when the radio was placed close to each other ($> 10\,\mathrm{m}$). However, when testing past this range and at any significant distance, the errors caused the received image to become unrecognisable. The type of error observed consists of contiguous bytes being lost occasionally, rather than frequent corruption of individual bytes as shown in 22.

Figure 22: Example of an image received with errors resulting in an unrecognisable image due to dropped bytes causing the image to shift at each error. Only a small proportion of the image is lost ($> 2\%$), represented by red pixels at the bottom and contiguous sections of the received image are error-free.

A chunk protocol was effective against this type of error while being simple to implement. It involves adding a header to signify the start of a chunk, followed by the chunk number and 400 bytes of pixel data as shown in 23. A 1600×1200 pixel image where each pixel is represented by one byte requires 4800 chunks to be sent in this implementation. The number of bytes per chunk is a trade-off between pixels lost per error and effective data rate.

A start of chunk marker of {`0x00, 0xFF, 0x00, 0xFF`} was chosen since the image data being transmitted are raw pixels, and it is unlikely for the image to contain pixels that are full or zero intensity, and even more unlikely for them to be adjacent to each other.

When an error occurs causing a string of bytes to be dropped, it causes the next chunk to not be encountered after 400 bytes. When this error occurs, the receiver searches for the next occurrence of the header and restarts receiving from that point. The chunks which were skipped have their pixels filled in the received image to prevent the error

causing the image to become unrecognisable.

The end of an image is signified by the ASCII string "EOFEOFEOFEOF". The start of chunk of the next image immediately starts after this string.

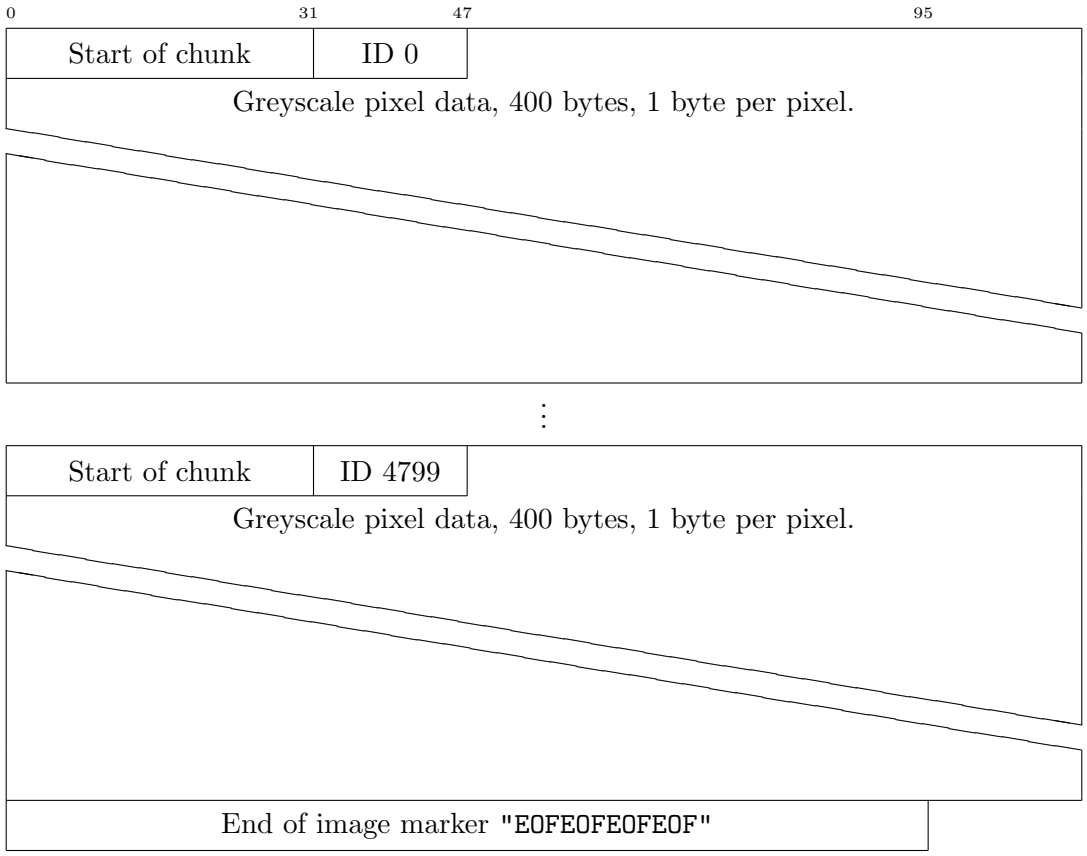

Figure 23: Image chunk protocol.

Software A Python script was developed for the DAQ which:

1. Opens the serial port `/dev/serial0` with the settings described in table 9.
2. Create and open a log file with a unique filename to dump the received bytes from the camera payload.
3. Periodically read a block of 2048 from the UART receive buffer and write the block to the file and UART output.
4. Every 3 seconds write a message to the UART output containing the current system time, the script's uptime and the number of UART errors.

This Python script is managed by a `systemd` service which reboots the script if it crashes.

The ground station is a laptop running Windows with an RFD900x connected to it over USB serial. There are two Python scripts on the laptop, the first saves the data from the radio to a file and prints any messages to the console.

1. Opens a serial port to the RFD900x with the UART settings of the ground RFD900x.
2. Create and open a log file to store the received bytes from the radio.
3. Periodically:

   Read the bytes in the serial buffer,

   Save the bytes to the log file,

   Find any start of message mark, and if encountered print all bytes until the end of message mark is received

A second script periodically reads the latest log file and splits it into images.

1. Allocate a `bytearray` for a full 1600×1200 pixel image.
2. Allocate a 1600×1200 `bytearray` where each byte is the state of each pixel (received or missing).
3. Read the whole file and strip all messages (bytes enclosed by the start and end of message markers).
4. Then find the indices of the end of image makers and split the file into several bytearrays, one for each image.
5. For each image bytearray:

   Find the next start of chunk

   Extract the chunk ID from the next two bytes.

   Extract image bytes starting from after the chunk ID to either the next header index, or the end of file if this doesn't exist.

   Add all bytes to the image byte array, starting at index `ID * 400` and set the state of the added pixels to "received".

   Repeat until the image array is full or there are no more bytes left in the image bytearray.

Results TODO: This might be better placed in the drone test section, but we'll have to deal with this redundant data.

TODO: Should it be hierarchical by system or by test?

This system was tested in the drone test at a distance of 120 m line of sight. The image received is shown in 24 with comparison to an image received without blocking:

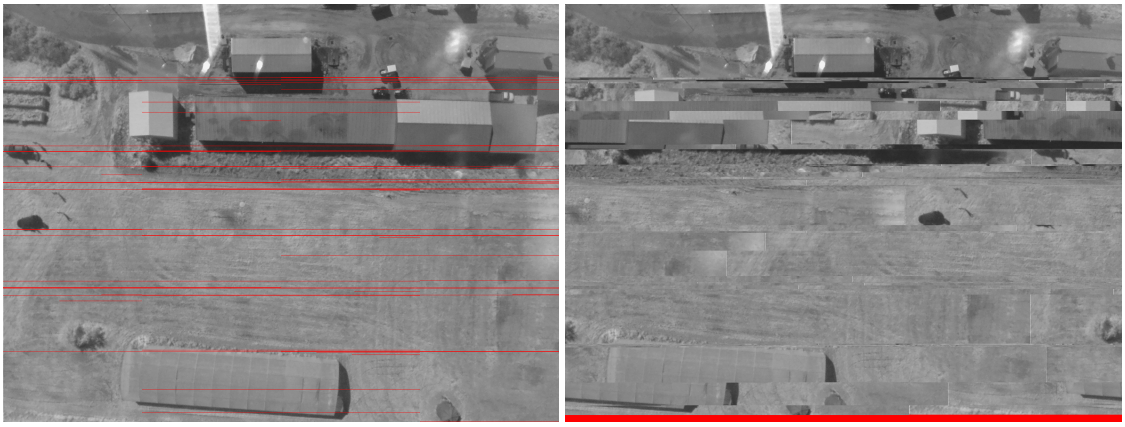

(a) (b)

Figure 24: Comparison of two image reception techniques. Image (a) used the blocking protocol with a block size of 400 pixels. Image (b) is an example of what the image would look like without the image blocking.

11.3 Accelerometer data acquisition system

Accelerometer PCB The accelerometer PCB (shown in figure 25) will contain both the ADXL375 and LSM6DSOX accelerometers and mount them to the chassis.

To maximise the resonant frequency of the assembly, the PCB is mounted on its flat side to the chassis and is fixed with four steel M3 bolts on each corner. Additionally, the dimensions of the PCB was minimised to 22 mm × 22 mm, which is the minimum dimension that can fit all components. Maximising the resonant frequency past the sampling frequency will minimise distortion of the response. The PCB is depicted in figure 25.

The PCB exposes one interrupt and chip select pin for each accelerometer, an SPI connection and 3.3 V power bus.

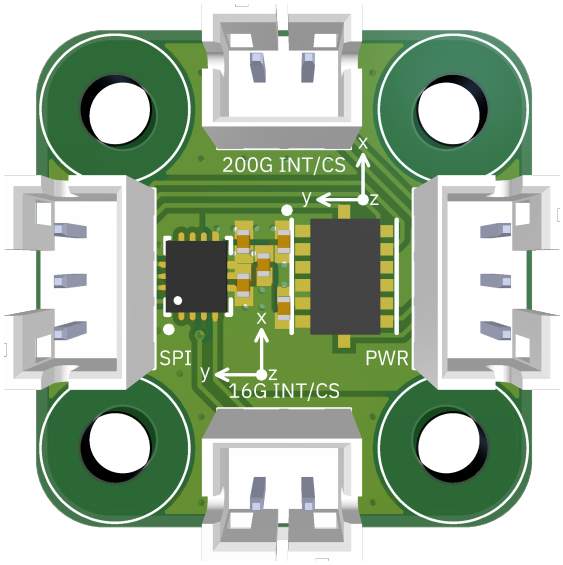

Figure 25: Accelerometer PCB.

Connection to DAQ The accelerometers are connected to the DAQ using the `SPI0` bus of the Pi Zero. The chip select ($\overline{\text{CS}}$) and interrupt (INT) pins are connected to GPIOs and are handled by software, therefore it is not necessary to only use the hardware SPI chip select/chip enable (CE) pins for all chip selects. This is depicted in figure 26. Although SPI requires more wiring, in the case of these sensors SPI has a higher clock speed compared to I^2C. For example, the LSM6DSO has supports the I^2C Fast Mode+ extension (FM+) which gives the I^2C bus a maximum clock rate of 1 MHz, but the SPI has a maximum clock speed of 10 MHz which is higher. SPI also has higher data rate for a given frequency than I^2C since I^2C adds additional flow control bits such as start, stop and acknowledgement bits.

This SPI bus is dedicated for only accelerometers to maximise the number of accelerometers connected, and is not shared with non-accelerometer peripherals.

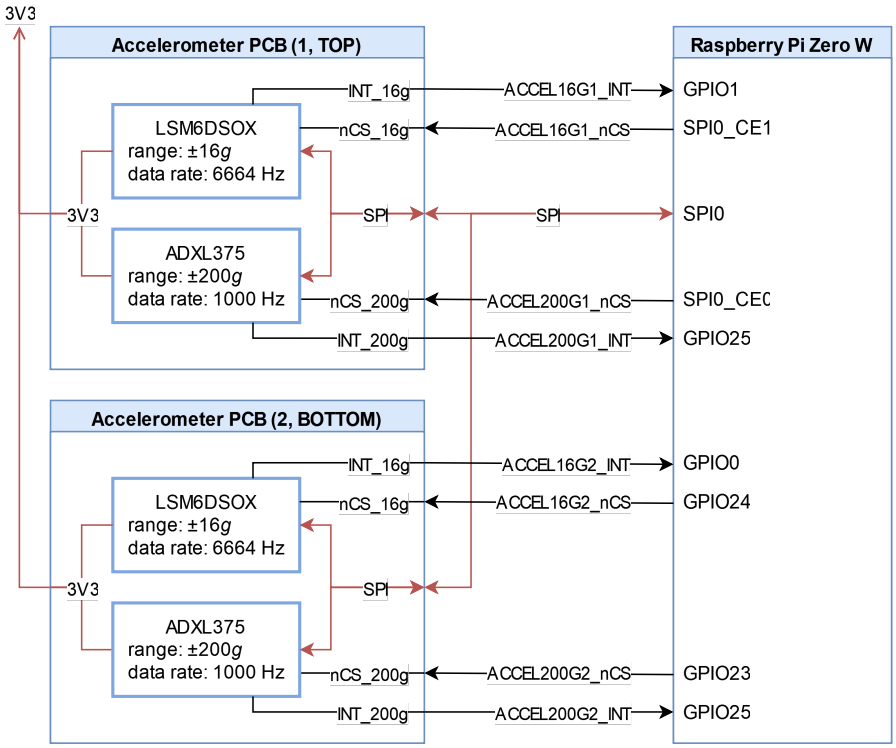

Figure 26: Block diagram of accelerometers and Pi Zero data acquisition system.

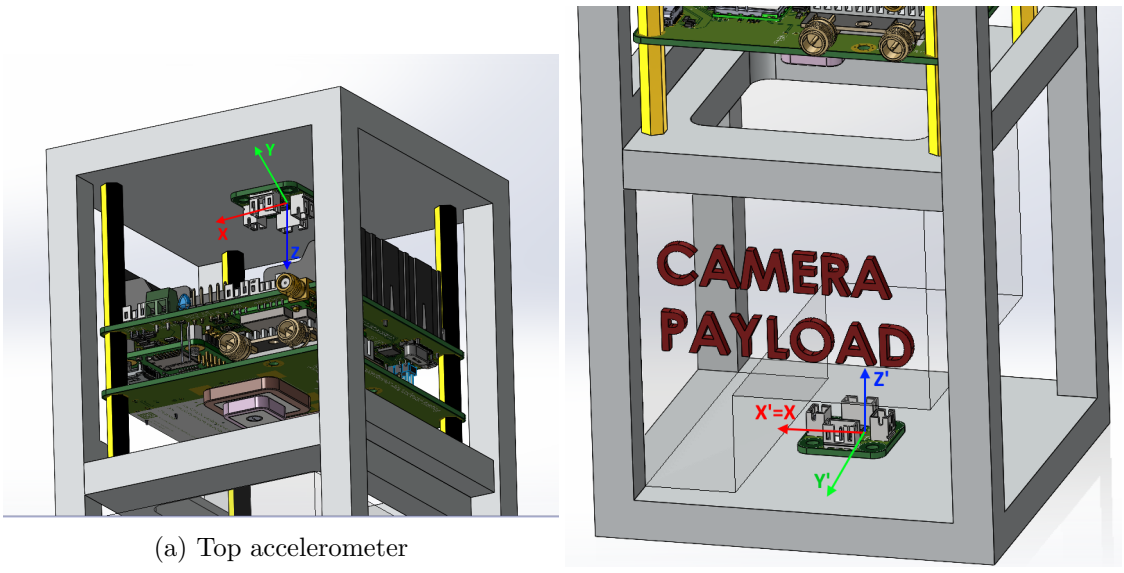

(a) Top accelerometer

(b) Bottom accelerometer.

Figure 27: Mounting positions of accelerometers on the CubeSat chassis. The top and bottom accelerometer share a common x axis but have opposite y and z axes.

LSM6DSOX software A C program is written to read values from the LSM6DSOX, package them into a binary flat file format and store them to disk. A C program is required since preliminary tests with a Python script with the same functionality resulted in 100% of the CPU being used to read from one accelerometer.

The `lsm6dso-pid` platform independent (PID) library was used to provide simple access to the registers of the accelerometer [49], in combination with WiringPi which provides bindings to GPIO, SPI and other peripherals on the Pi [50].

To maximise sampling rate and minimise CPU usage, the accelerometer is operated using the FIFO and interrupt features.

Samples from the accelerometer are stored in binary flat file format, consisting of the `struct datapoint` for each 3-axis sample. A header of `0x59` is used which signifies the start of a sample. The type field is set to either 1 for accelerometer samples or 2 for gyroscope samples.

```
struct datapoint
{
    char header;
    char type;
    float x;
    float y;
    float z;
};
```

To improve reliability, the LSM6DSOX program contains a watchdog, implemented using a POSIX timer, which restarts and re-initialises the accelerometer if no samples have been received for 1 s. The process is managed by a `systemd` service which initialises the program on system boot and restarts the program if it crashes.

The following is a description of the program TODO:

1. Read the first argument, which describes the sensor that the process will manage (1 or 2), and open the appropriate SPI bus using WiringPi.
2. Open a new unique binary file to store the samples to.
3. Create a watchdog POSIX timer and debug printing POSIX timer.
4. Attach the FIFO read interrupt handler on the interrupt pin.
5. Initialise the LSM6DSOX by issuing the following commands:
6. Ensure the `WHO_AM_I` register matches the expected value,
7. Software reset the device,
8. Wait for the device to be reset,
9. Disable the I^3C interface,

10. Enable block data update,
11. Set the scale for the accelerometer to 16 g, the maxmium full scale possible,
12. Set the sampling rate to 6666 Hz and the batching rate to 12.5 Hz,
13. Set the FIFO to continuous mode (old samples are automatically discarded),
14. Set FIFO watermark level to 384 samples,
15. Set interrupt pin 1 to pulse on FIFO watermark being reached (this results in a pulse being generated on the INT1 pin when a large amount of data is present in the FIFO to be read, resulting in the interrupt handler being triggered.),

The interrupt handler has the following functionality and is based off sample code from the LSM6DSOX PID library [49]:

1. Immediately reset the watchdog timer to 1 second (to prevent it triggering since a read is started)
2. Read the number of samples in the FIFO. For each sample:
3. Read the sample's tag and if it is accelerometer data then read the sample from the FIFO into a 6-byte array
4. Convert each of the three axes (represented by two byte words) to mg.
5. Store the reading in a struct with the correct header and type and write to the log file.
6. For debug reasons, print the current sample every 3332 samples (every half second).

Unpacking data for data analysis The accelerometer binary files are read on a PC using a Python script which uses the `struct` library to unpack the file and convert it to a traditional comma-separated values (CSV) file.

11.4 GNSS tracking

11.5 Downlink

12 High-Power Rocket

A custom rocket named UNO was designed and built by another project member from scratch, it has a height of 290 cm, diameter of 16.3 cm and a dry mass of 14.42 kg without a motor. It was designed to fly with an M impulse class motor, however due to changes in United States export regulations it was not possible to obtain this motor in the time of this research, and therefore it was only possible to launch with a K impulse class motor which has about 1/10th of the total impulse of the N motor as shown in table **??**.

Total impulse [N s]	Motor impulse class
160.01 - 320.00	H
320.01 - 640.00	I
640.01 - 1,280.00	J
1,280.01 - 2,560.00	K
2,560.01 - 5,120.00	L
5,120.01 - 10,240.00	M
10,240.01 - 20,560.00	N
20,560.01 - 40,960.00	O
40,960.01 - 81,920.00	P
81,920.01 - 163,840.00	Q

Table 10: Rocket motor impulse classes [51]

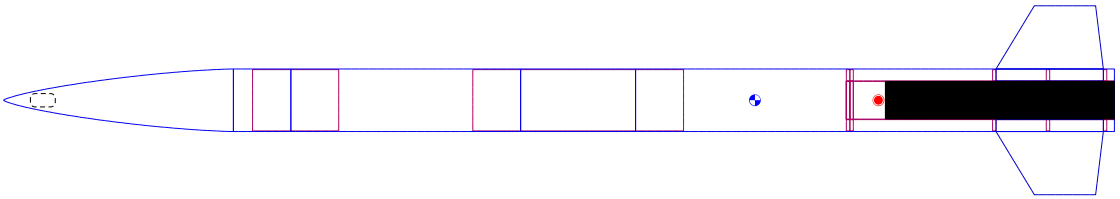

Figure 28: OpenRocket diagram of UNO.

12.1 Simulation

The rocket was simulated using OpenRocket [52], [53], an open-source simulator which can predict parameters such as stability and acceleration based on empirical methods which use the rocket's shape and basic environment parameters such as constant wind [53], [54]. OpenRocket is used to ensure the rocket design is stable throughout launch and flight, which is important to ensuring the CubeSat payload does not become damaged by this qualification method. However, as it uses a simple empirical model of the flight, it was not designed to model the effect of the motor and aerodynamic forces on the vibration environment in the rocket. It also does not simulate pyroshock events, instead modelling parachute deployment events as simple changes in the aerodynamics of the rocket [53].

12.1.1 Flight profile

As shown in **??** the rocket reaches an apogee of 413 m at 9.74 s and the total flight time is 30 s.

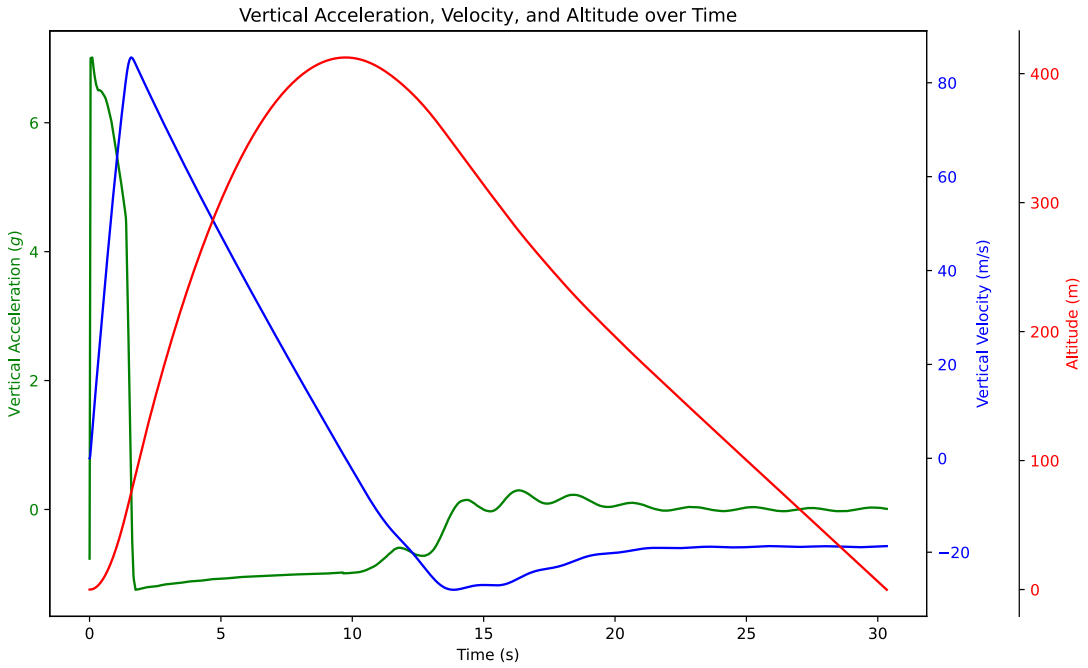

Figure 29: Flight profile of UNO using a K1100T motor. Simulated in OpenRocket.

12.1.2 Stability

As shown in figure **??**, the stability is above 2.0 calibres for the coast and launch phase, which is a rule of thumb to ensure the rocket is stable and will not veer off course [23]. The short moment of stability below 2.0 occurs when the rocket reaches apogee, which is not an issue since the parachutes are immediately deployed at this point.

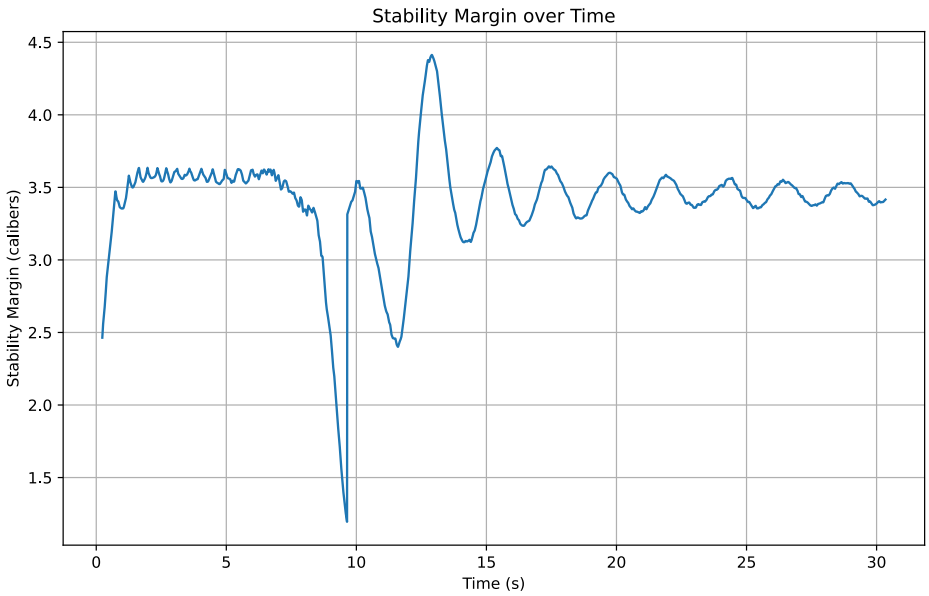

Figure 30: Stability of UNO using a K1100T motor. Simulated in OpenRocket.

12.1.3 Acceleration

As stated, since OpenRocket does not model the vibration environment in the rocket and models the rocket as one solid body, only the acceleration of the whole rocket can be modelled. Pyroshock events are not modelled by OpenRocket. The launch phase lasts only 1.6 s and has a high average acceleration of 5.77 g, as shown in **??**. During the coast phase, the rocket is decelerated by gravity as expected and after parachute deployment the rocket only has a small deceleration force.

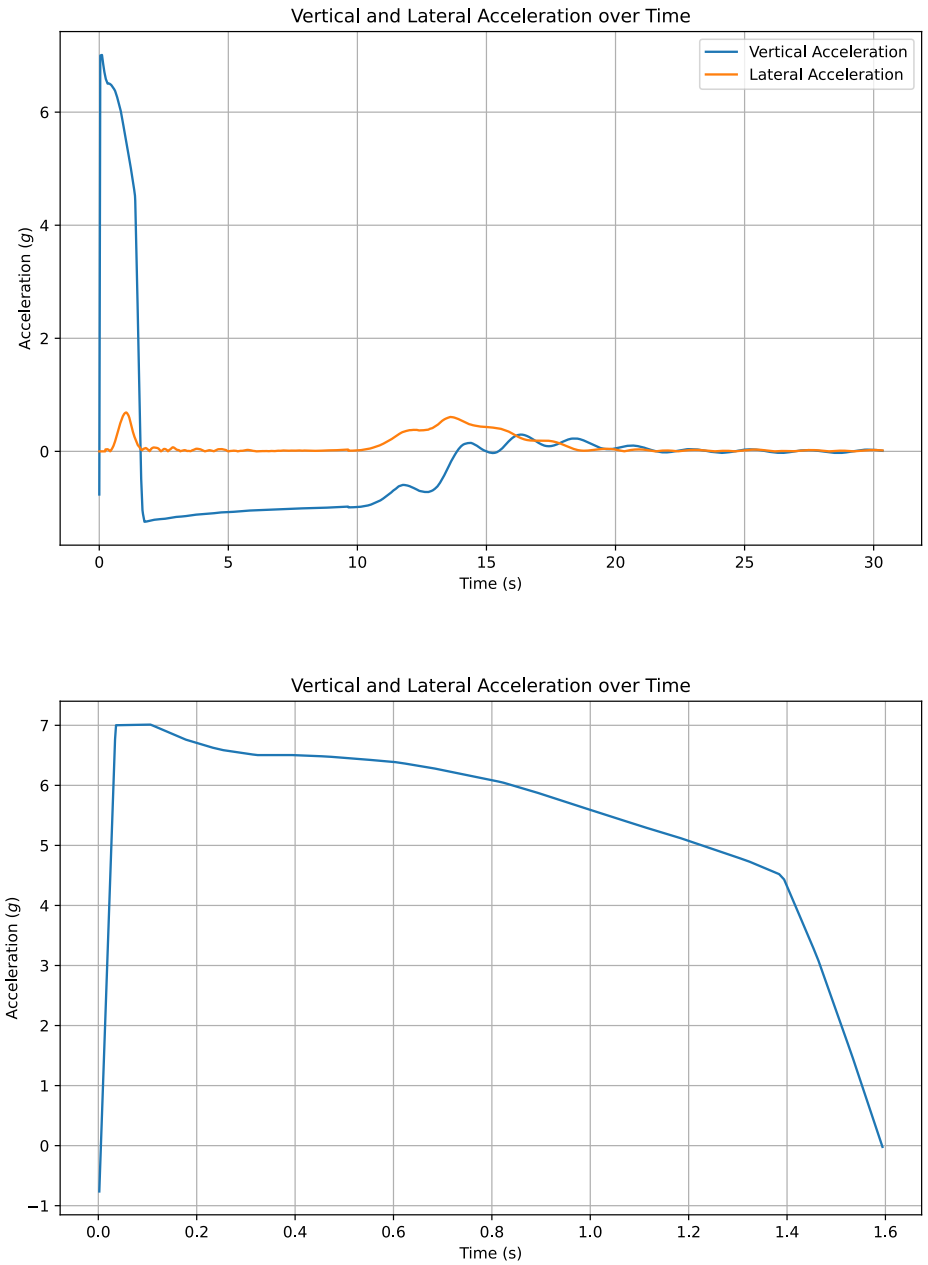

Figure 31: Acceleration of UNO using a K1100T motor over (top) the whole flight and (bottom) the thrust phase. Simulated in OpenRocket.

13 Testing

13.1 Vibration table testing

13.1.1 AVI vibration table test setup

13.2 Rocket test

TODO: Explain setup in rocket

13.3 Drone tests

13.3.1 First test

13.3.2 Second test

13.3.3 Third test

13.4 Freezer test

13.5 Oven test

14 Data collection and analysis

The system will be used for the vibration tests on a shaker table, and the rocket test. The data will be recorded as a time series on the OBDH memory. The time series data will be transformed into the frequency domain since existing studies have presented frequency domain plots to present and analyse the response of the system to a test [13], [20]. For the rocket test, the analysis will be split over the several phases of flight - launch, thrust, coast and parachute deployment events, since the forces involved are different in all of these phases.

14.1 Shock

14.1.1 Vibration table results

14.1.2 HPR results

14.1.3 Comparison of methods

In the launch and parachute deployments, where pyrotechnics are ignited, an analysis of the shock response spectrum will be performed. This will involve creating the shock response spectrum for the rocket test and shaker table tests, then comparing the slope up to 1 kHz. If the rocket test SRS slope is on the same order of magnitude as the gradient found in [24] for other low explosives, and it is less than the slope of the SRS from the shaker table tests, then this will show that rocket testing is not an adequate qualification method for shock.

14.2 Random

14.2.1 Vibration table results

14.2.2 HPR results

14.2.3 Comparison of methods

The coast phase, where the rocket motor has burnt out but is still approaching apogee, will be compared to the random vibration test. The random response spectrum will be compared to the spectrum of the rocket test to check how uniformly distributed the rocket test is.

14.3 Quasi-static acceleration

14.3.1 Vibration table results

14.3.2 HPR results

14.3.3 Comparison of methods

The boost phase will be compared to the quasi-static acceleration tests on the shaker table. It is expected that the acceleration force on the HPR will be greater than those experienced on the launch vehicle, however the key characteristic - a peak in acceleration over a narrow frequency band - should be the same.

15 Conclusions

15.0.1 Conclusions

TODO: A data acquisition system was developed, blah blah high power rocket bad shaker table good

15.1 Future work

TODO: Blah blah do test on hpr rocket with larger motor, do test on launch vehicle
Hardware changes for a future revision of the data acquisition system include:

- Use Raspberry Pi Zero 2W instead of Zero W since it has more cores.
- Machine a heatsink to connect all chips on the Pi Zero module to the chassis or heatsink to ensure better thermal performance [46].
- Power switch should be through a resistor to prevent case where battery short circuit causes wire fire.
- Batteries should be spot welded to tabs that are soldered fixed to the PCB to make pack resistant to random vibration.
- Investigate the use of fault-tolerant compression algorithms for the downlink.

16 References

[1] R. P. Welle, "Overview of cubesat technology," *Handbook of Small Satellites: Technology, Design, Manufacture, Applications, Economics and Regulation*, pp. 1–17, 2020.

[2] J. Bouwmeester, A. Menicucci, and E. K. Gill, "Improving cubesat reliability: Subsystem redundancy or improved testing?" *Reliability Engineering & System Safety*, vol. 220, p. 108 288, 2022.

[3] S. Gordon and D. L. Kern, "Benefits of spacecraft level vibration testing," in *Aerospace Testing Seminar*, 2015.

[4] L. K. Slongo, J. G. Reis, D. Gaiki, P. V. H. Seger, S. V. Martínez, B. V. B. Eiterer, T. G. Pereira, M. B. Neto, M. dos Santos Frata, H. D. Hamisch, *et al.*, "Pre-flight qualification test procedure for nanosatellites using sounding rockets," *Acta Astronautica*, vol. 159, pp. 564–577, 2019.

[5] T. Ludovico, "Targeting low earth orbit vegetation indexing for home grown sensing," Master's thesis, The University of Western Australia, 2024.

[6] N. Nath and G. S. Aglietti, "Study the effect of tri-axis vibration testing over single-axis vibration testing on a satellite," in *2022 IEEE Aerospace Conference (AERO)*, IEEE, 2022, pp. 1–10.

[7] D. T. Pierce, "Development of a rocket test platform capable of delivering standard dimension payloads to near-space altitudes," Ph.D. dissertation, Monterey, CA; Naval Postgraduate School, 2019.

[8] M. G. Mariano, F. E. Morsch, M. S. Vega, D. M. A. M. Pio, S. L. Oriel, S. L. Kessler, and B. E. Augusto, "Qualification and validation test methodology of the open-source cubesat floripasat-i," *Journal of Systems Engineering and Electronics*, vol. 31, no. 6, pp. 1230–1244, 2020. DOI: 10.23919/JSEE.2020.000103.

[9] G. Minelli, L. Magallanes, N. Weitz, D. Rigmaiden, J. Horning, J. Newman, M. Scott, S. Brady, C. Watkins, J. Christensen, *et al.*, "The mobile cubesat command and control (mc3) ground station network: An overview and look ahead," 2019.

[10] NASA Goddard Space Flight Center, *General Environmental Verification Standard (GEVS) for GSFC Flight Programs and Projects*, NASA Technical Standard, Document date: April 28, 2021., NASA Goddard Space Flight Center, 2021. [Online]. Available: {https://standards.nasa.gov/standard/GSFC/GSFC-STD-7000}.

[11] M. Cho, H. Masui, T. Hatamura, S. Horii, S. Obata, *et al.*, "Overview of nanosatellite environmental tests standardization project: Test campaign and standard draft," 2012.

[12] C. D. Brown 1930, *Elements of spacecraft design*, English, ser. AIAA education series. Reston, VA: American Institute of Aeronautics and Astronautics, 2002, ISBN: 978-1-60086-051-5 1-60086-051-6 978-1-60086-179-6 1-60086-179-2. [Online]. Available: https://doi.org/10.2514/4.861796.

[13] C. Nieto-Peroy and M. R. Emami, "Cubesat mission: From design to operation," *Applied Sciences*, vol. 9, no. 15, p. 3110, 2019.

[14] G. S. Aglietti, M. Remedia, M. Appolloni, and A. Kiley, "Spacecraft structure model validation and test philosophy," *AIAA Journal*, vol. 57, no. 5, pp. 2109–2122, 2019.

[15] W. Rawson and E. G. Lightsey, "Best practices and considerations for planning and conducting integration of university cubesats,"

[16] Z. S. Decker, "A systems-engineering assessment of multiple cubesat build approaches," Ph.D. dissertation, Massachusetts Institute of Technology, 2016.

[17] J. Dickens, M. Wittbrodt, M. Gate, L. Li, and A Stroeve, "Coupled loads analysis accuracy from the space vehicle perspective," *Acta Astronautica*, vol. 48, no. 1, pp. 21–28, 2001.

[18] D. Casalino, S. Santini, M. Genito, and V. Ferrara, "Rocket noise sources localization through a tailored beam-forming technique," *AIAA journal*, vol. 50, no. 10, pp. 2146–2158, 2012.

[19] L. J. Bement and M. L. Schimmel, "A manual for pyrotechnic design, development and qualification," Tech. Rep., 1995.

[20] National Aeronautics and Space Administration, *Pyroshock test criteria*, NASA Technical Standard, National Aeronautics and Space Administration, 2011. [Online]. Available: {https://s3vi.ndc.nasa.gov/ssri-kb/static/resources/NASA-STD-7003A.pdf}.

[21] G. Seibert and B. T. Battrick, *The history of sounding rockets and their contribution to European space research*. ESA Publications division Noordwijk, 2006.

[22] B. Pont, J. Beurskens, J Dalderup, P. Dolron, J Gubbels, J Horandel, R. Jordans, H. Pourshaghaghi, D Szálas-Motesiczky, T. v. Vliet, *et al.*, "Rexus-25 rocket flight of a cubesat cosmic-ray detector," 2019.

[23] M. Canepa, *Modern high-power rocketry*. Trafford Publishing, 2005, vol. 2.

[24] J. Wang, X. Ren, X. Li, Y. Wen, L Cheng, and Q Guo, "Numerical simulation of the effect of combustion characteristics of main charges on the output shock of a typical igniter," in *Journal of Physics: Conference Series*, IOP Publishing, vol. 2478, 2023, p. 072 024.

[25] N. Meirambekuly, B. A. Karibayev, T. A. Namazbayev, G.-G. A. E. Ibrayev, S. O. Orynbassar, S. A. Ivanovich, and A. A. Temirbayev, "A high gain deployable l/s band conical helix antenna integrated with optical system for earth observation cubesats," *IEEE Access*, vol. 11, pp. 23 097–23 106, 2023. DOI: 10.1109/ACCESS.2023.3253556.

[26] P Falstad, "Falstad circuit simulator," *https://falstad.com/circuit/circuitjs.html (accessed Oct. 14 2024)*,

[27] M. Giesselmann and V. Roy, "Modeling of power supplies for power modulators with ltspice," *IEEE Transactions on Dielectrics and Electrical Insulation*, vol. 26, no. 2, pp. 508–514, 2019.

[28] Analog Devices, *Ltspice help*, `https://ltwiki.org/files/LTspiceHelp.chm/html/SPICE.htm` (accessed Oct. 8, 2024), 2022.

[29] K Jagdale, M Munjal, P Kurrey, A Wakode, P Lohiya, P Shrivas, A Sikka, S Bhansali, A Kejriwal, A Vadladi, *et al.*, "Sanket—technology demonstration of antenna deployment system on pslv stage 4 orbital platform," in *Advances in Small Satellite Technologies: Proceedings of National Conference on Small Satellite Technology and Applications, NCSSTA 2020*, Springer, 2023, pp. 87–95.

[30] Australian Youth Aerospace Association, *2024 aurc rocket specifications*, version Draft A, `https://aurc.ayaa.com.au/wp-content/uploads/2023/12/2024-AURC-Rocket-Specifications-Draft-A.pdf` (accessed Oct. 15, 2024), 2023.

[31] V. Knap, L. K. Vestergaard, and D.-I. Stroe, "A review of battery technology in cubesats and small satellite solutions," *Energies*, vol. 13, no. 16, p. 4097, 2020.

[32] A. D. Pathak, S. Saha, V. K. Bharti, M. M. Gaikwad, and C. S. Sharma, "A review on battery technology for space application," *Journal of Energy Storage*, vol. 61, p. 106 792, 2023.

[33] F. Krause, J.-P. Ruiz, S. Jones, E. Brandon, E. Darcy, C. Iannello, and R. Bugga, "Performance of commercial li-ion cells for future nasa missions and aerospace applications," *Journal of The Electrochemical Society*, vol. 168, no. 4, p. 040 504, 2021.

[34] G. M. Marcelino, E. Morsch Filho, S. V. Martinez, L. O. Seman, and E. A. Bezerra, "In-orbit preliminary results from the open-source educational nanosatellite floripasat-i," *Acta Astronautica*, vol. 188, pp. 64–80, 2021.

[35] Samsung SDI Co., Ltd., "Specification of product: Lithium-ion rechargeable cell for power tools (model: Inr18650-25r)," Tech. Rep., version 1.0, 2014.

[36] Raspberry Pi Ltd, *Raspberry pi hardware - raspberry pi hardware*, `https://www.raspberrypi.com/documentation/computers/raspberry-pi.html` (accessed Oct. 15, 2024), 2024.

[37] RF Design, *Rfd900x and rfd868x radio modem datasheet*, `https://files.rfdesign.com.au/Files/documents/RFD900x%20DataSheet%20V1.2.pdf` (accessed Oct. 15, 2024), 2020.

[38] u-blox, *Neo-m9n-00b - data sheet*, `https://content.u-blox.com/sites/default/files/NEO-M9N-00B_DataSheet_UBX-19014285.pdf` (accessed Oct. 15, 2024), 2023.

[39] STMicroelectronics, *LSM6DSO: iNEMO inertial module: always-on 3D accelerometer and 3D gyroscope*, STMicroelectronics, 2019. [Online]. Available: `https://www.st.com/resource/en/datasheet/lsm6dso.pdf`.

[40] Analog Devices, *Adxl375 data sheet*, https://www.analog.com/media/en/technical-documentation/data-sheets/ADXL375.PDF (accessed Oct. 15, 2024), 2014.

[41] MaxLinear, *Sp3485 data sheet*, https://www.maxlinear.com/ds/sp3485.pdf (accessed Oct. 15, 2024), 2021.

[42] ——, *Xr20m1172 two channel i2c/spi uart with 64-byte fifo*, https://www.maxlinear.com/ds/xr20m1172.pdf (accessed Oct. 15, 2024), 2022.

[43] Texas Instruments, *Tps61022 8-a boost converter with 0.5-v ultra-low input voltage*, D, https://www.ti.com/lit/ds/symlink/tps61022.pdf (accessed Oct. 15, 2024), 2021.

[44] Advanced Monolithic Systems, Inc., *Ams1117 1a low dropout voltage regulator*, http://www.advanced-monolithic.com/pdf/ds1117.pdf (accessed Oct. 15, 2024), 2007.

[45] E. Upton and G. Halfacree, *Raspberry Pi user guide*. John Wiley & Sons, 2016.

[46] S. M. Guertin, "Raspberry pis for space guideline," *NASA: Washington, DC, USA*, 2022.

[47] Department of Infrastructure, Transport, Regional Development, Communications and the Arts, *Radiocommunications (low interference potential devices) class licence 2015*, https://www.legislation.gov.au/F2015L01438/latest/text (accessed Oct. 15, 2024), 2015.

[48] A. Cratere, L. Gagliardi, G. A. Sanca, F. Golmar, and F. Dell'Olio, "On-board computer for cubesats: State-of-the-art and future trends," *IEEE Access*, 2024.

[49] STMicroelectronics, *Lsm6dsox-pid*, https://github.com/STMicroelectronics/lsm6dsox-pid (accessed Oct. 15, 2024), 2024.

[50] Grazer Computer Club, *Wiringpi library*, https://github.com/WiringPi/WiringPi (accessed Oct. 15, 2024), 2024.

[51] National Fire Protection Association, *NFPA 1127 Code for High Power Rocketry*, 2018 edition. NFPA, 2018.

[52] Sampo Niskanen and others, *Openrocket simulator*, https://openrocket.info/index.html (accessed Oct. 10, 2024), 2024.

[53] S. Niskanen, "Development of an open source model rocket simulation software," Master's thesis, Aalto University, Espoo, 2009. [Online]. Available: https://github.com/openrocket/openrocket/releases/download/Development_of_an_Open_Source_model_rocket_simulation-thesis-v20090520/Development_of_an_Open_Source_model_rocket_simulation-thesis-v20090520.pdf.

[54] W. Brown, M. Wiesneth, T. Faust, N. Huynh, C. Montalvo, K. Lino, and A. Tindell, "Measured and simulated analysis of a model rocket," *Proceedings of the Institution of Mechanical Engineers, Part G: Journal of Aerospace Engineering*, vol. 233, no. 4, pp. 1397–1411, 2019. DOI: 10.1177/0954410017752730. eprint: https://doi.org/10.1177/0954410017752730. [Online]. Available: https://doi.org/10.1177/0954410017752730.

17 Appendix

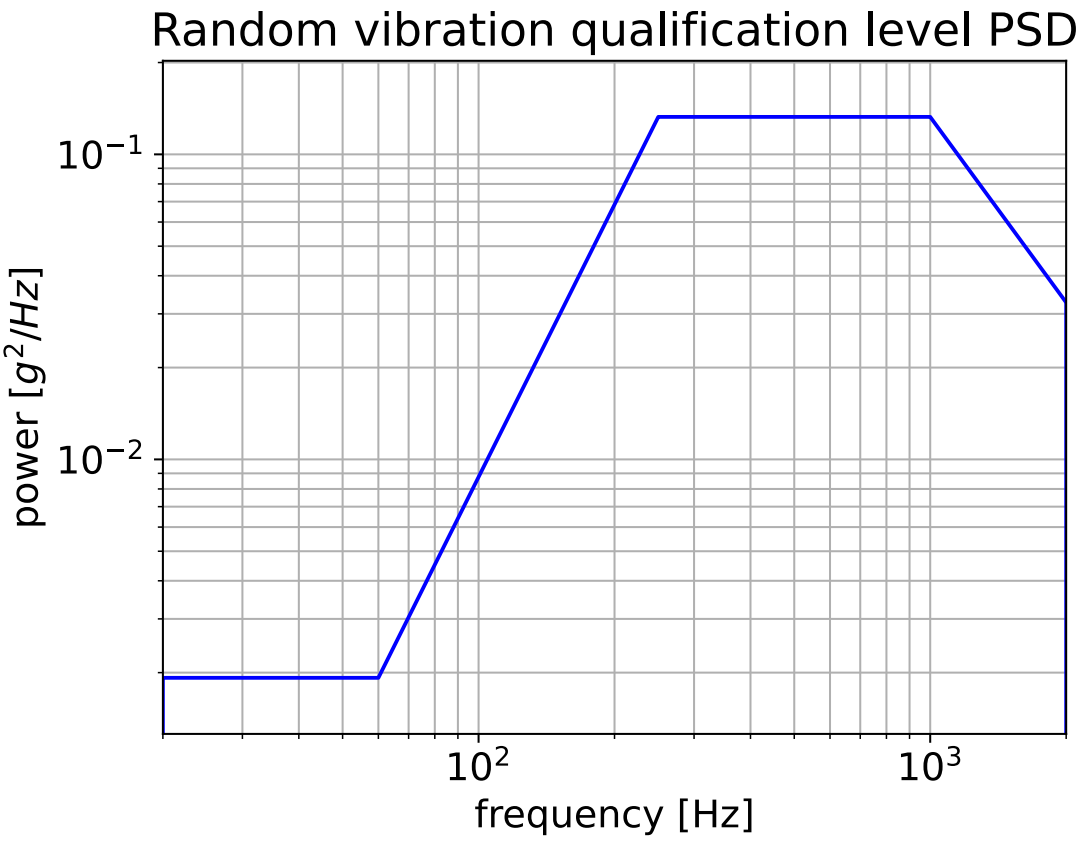

Figure 15: IIST recommended random vibration test profile for qualification of CubeSat for launch on POEM (profile defined in 4).